RESEARCH ARTICLE

An integrated approach based on HFE-D, GIS techniques, GQI_{SWI}, and statistical analysis for the assessment of potential seawater intrusion: coastal multilayered aquifer of Ghaemshahr-Juybar (Mazandaran, Iran)

Tahereh Azari[1] · Mahmoud Mohammad Rezapour Tabari[1,2]

Abstract

The overexploitation of coastal aquifers is one of the important reasons for the salinity of groundwater due to seawater intrusion (SWI). This study assesses the hydrochemical changes of the Ghaemshahr-Juybar (GH.-J.) plain. For this purpose, specific statistical methods, modified Piper diagram groundwater quality indicators ($GQI_{Piper(mix)}$ and $GQI_{Piper(dom)}$), groundwater quality index specific to seawater intrusion (GQI_{SWI}), and hydrochemical facies evolution diagram (HFE-D) along with GIS (Geographic Information System) techniques were applied to identify the spatiotemporal changes of salinity in coastal multilayer alluvial aquifer. The results show that the chemical composition in the GH.-J. aquifer is basically controlled by three main factors: (1) Caspian SWI and fossil saltwater penetration from an underlying layer, (2) reverse cation exchange process, and (3) feeding by domestic sewage, agricultural activities, and use of nitrate chemical fertilizers. The investigation of the hydrogeochemical facies evolution process shows that due to the reduction of extraction from wells, saltwater infiltration has significantly decreased. Therefore, according to the geological and lithological conditions of the aquifer and exposure to seawater, it is possible to prevent the entry of saltwater from the confined aquifer into the unconfined aquifer and the saltwater intrusion by developing well optimal operation policies in order to control withdrawal from semi-deep wells and the elimination of deep wells. This practical approach to managing the salinity of coastal aquifers is suitable for the allocating groundwater resources and for use in the development of aquifer simulation models.

Keywords Saltwater intrusion · Coastal aquifer · Principal component analysis (PCA) · Groundwater quality index (GQI) · Hydrochemical facies evolution diagram (HFE-D) · Ghaemshahr-Juybar aquifer

Introduction

In arid and semi-arid regions, groundwater is one of the most critical sustainable sources of freshwater supply in domestic, agricultural, industrial, and other sectors (Chitsazan et al. 2017).

✉ Mahmoud Mohammad Rezapour Tabari
mrtabari@umz.ac.ir

1 Department of Civil Engineering, Faculty of Engineering and Technology, University of Mazandaran, Mazandaran, Iran

2 Water Resources Research in the Area of Marine, Coastal and Wetlands Core, University of Mazandaran, Babolsar, Iran

In recent years, many groundwater sources, especially aquifers located in the coastal belt, have been exposed to seawater intrusion (SWI) due to the increasing water demands resulting from the population growth and agricultural development (Chandra Pal et al. 2022; Desai and Desai 2012; Singh 2015).

The seawater intrusion, besides causing pollution in the aquifer freshwater, can leave irreparable effects on the condition of cultivable soil and the natural ecosystem of coastal areas. Failure to properly recognize and manage this phenomenon in the long term will destroy the stable conditions of the aquifer, which is one of the main components in the economic improvement of coastal communities (Siddha and Sahu 2020).

The development and increase of withdrawals by operation wells disturb the natural balance between salt and

freshwater in unconfined coastal aquifers. This leads to a decrease in the freshwater thickness and the intrusion of saline water, resulting in an increase in salinity in groundwater resources (Asare et al. 2021; Tabari and Abyar 2022). According to the studies of Abd-Elaty et al. (2021), reducing the pumping from unconfined aquifers, increasing aquifer recharge using treated agricultural wastewater, and abstraction, desalination, and recharge (ADR) system can control the SWI. In confined and perched coastal aquifers, due to the existence of confining layers and clay lenses, hydrogeological processes are more complex, and geochemical processes lead to the SWI from the underlying layers (Sahour et al. 2020). Based on previous studies, several factors lead to the creation and development of salinity in coastal aquifers: the decrease in the groundwater level; the increase in the level of seawater as a result of climate change, dissolution of rocks, weathering, and ion exchange; and the rise of paleo-salinewater as a result of significant pumping of exploitation wells or anthropogenic factors such as the entry of agricultural, industrial, and urban wastewaters (Barkat et al. 2021; Guo et al. 2021; Hajji et al. 2021; Larsen et al. 2017; Mtoni et al. 2013). Therefore, knowing the sources and mechanisms in the salinization process of coastal aquifers is of great importance for effective and sustainable management. In order to investigate and monitor of the saltwater intrusion phenomenon in coastal aquifers, different approaches have been used in previous studies. Among them, the following studies can be mentioned: investigating factors affecting groundwater salinity and its modeling using multivariate regression method to make a salinity map in the Caspian southern coasts by Gholami et al. (2009). The results showed that the quality of recharged surface water (agricultural wastewater) is the most important factor of groundwater salinity in this region, and the decrease in rainfall from west to east of Mazandaran Province has led to an increase in the salinity of aquifer samples. In 2016, to delineate and evaluate the processes governing the intrusion of Mahrlu Lake saline water into the coastal aquifer located in its southern part, Jahanshahi and Zare (2016) examined the groundwater type, iso EC maps, iso ions and ion exchanges in the mixing process of salt and freshwater, and depth variations of salinity in coastal wells. The time variation of the physical and chemical parameters of groundwater showed that saline water has moved upward from the bottom of the aquifer and destroyed the groundwater quality due to overexploitation and the change of hydraulic gradient from the lake to the aquifer. Also, geological formations and evaporation from shallow groundwater were effective in increasing the salinity of the aquifer. The spatiotemporal distribution of salinity in Caspian Sea coastal aquifers using geostatistical analysis by Amiri-Bourkhani et al. (2017) was investigated. The results indicate an increase in the salinity of aquifers from south to north and west to east. Increasing agricultural land in

the central and eastern parts and the long-term operation of groundwater resources, the percolation of agricultural wastewater, the high concentration of population, and, as a result, increasing extraction of groundwater have been introduced as the main factors of the salinity and SWI. Kanagaraj et al. (2018) used geophysical, geochemical, and stable isotope techniques to determine hydrogeochemical processes and the effect of SWI in coastal aquifers south of Chennai, India. The results showed that agricultural activities and geotechnical processes are the causes of SWI. Sahour et al. (2020) investigated the distribution of salinity in coastal aquifers of the southern Caspian Sea using hydrogeological and hydrological data, statistical techniques, and machine learning. Their findings indicate that the transmissibility of the aquifer is the most critical parameter affecting the salinity of the groundwater. Using classical integration methods and multivariate statistical analysis, Khairy and Janardhana (2021) investigated the qualitative details of the aquifer in terms of salinity and its controlling factors. Using quantitative indicators, Sarkar et al. (2021) measured the intensity of SWI in the coastal region of West Bengal, India, and traced its dominant mechanism. Accordingly, frequent storm surges, rising seawater, overexploitation of groundwater, and silicate weathering were considered as the main factors of SWI. Le et al. (2020) identified the spatial distribution and hydrogeochemical evolution process of saline water in a coastal four-layer aquifer in Southern Vietnam using the HFE-D diagram and GIS. Ghezelsofloo et al. (2021) evaluated the intrusion of saline water into the coastal aquifer wells of Kordkuy with hydrogeochemical methods and geophysical studies. The hydrogeochemical evolution of the Rhodope coastal aquifer based on the analysis of qualitative samples and multivariate statistical methods by Tziritis et al. (2023) was studied.

The surveys of relevant prior literature, as mentioned in the previous section, show that the approaches used in SWI evaluation can be divided into several categories: determination of the origin of salinity based on the hydrogeochemical facies governing the aquifer using diagrams like Piper, hydrochemical facies evolution (HFE), Stiff, Durov, and Gibbs (Biswas et al. 2023; Ghezelsofloo et al. 2021; Gimenez-Forcada 2010; Kelepertzis et al. 2023; Le et al. 2020; Li et al. 2020), multivariate statistical analysis and the use of correlation coefficients and relationships between qualitative parameters (Amiri et al. 2021; Parisi et al. 2023; Tziritis et al. 2023), geophysics-based methods (Kouzana et al. 2010; Kura et al. 2014; Meyer et al. 2019), the use of isotopes in identifying the origin and age of saltwater in the aquifer (Carol et al. 2009), and spatiotemporal investigation of salinity intrusion using GIS and modeling (Abba et al. 2023; Dhar and Datta 2009; Kawo and Karuppannan 2018; Xiong et al. 2023). The studies by the authors of this article indicate that the use of statistical methods and the analysis

of chemical facies, employing qualitative samples, have become more prevalent in evaluating saltwater intrusion in coastal aquifers. The integrated utilization of the capabilities of the mentioned approaches allows for the accurate identification of the causes of salinity and the determination of the processes governing the aquifer's exposure to salinity. Despite investigating different approaches to SWI assessment in the coastal aquifers, it is essential to study the status of Caspian Sea intrusion in the coastal aquifer of northern Iran and its effects. The Caspian Sea is the largest closed lake in the world, and its level is 27 m below the level of the open seas (Khairy and Janardhana 2013). Mazandaran Province in the northern coastal region of Iran, located on the southern shore of the Caspian Sea, due to having diverse vegetation and moderate climate, is considered one of the important areas in terms of the production of agricultural products (rice farms and citrus gardens) and tourism (Heidari Cherati 2020). In this province, the depth of the groundwater table level is less than 10 m, and for this reason, these water resources are exposed to salinity (Gholami et al. 2009).

This plain region has 600,210 ha of cultivated land (agricultural (74%) and garden (26%)). The strategic products of this region are rice and citrus fruits (with 36% and 44% of the IRAN production, respectively), which have been assigned the first rank of production in both products (Jehad 2020). In this area, the Ghaemshahar-Juybar (GH.-J.) aquifer is considered one of the six potential aquifers in the vicinity of the Caspian Sea, with suitable freshwater reserves. More than 10% of agricultural land in Mazandaran Province is located in this aquifer (Motevalli et al. 2019). The pressure on the groundwater resources of this aquifer has increased due to the decrease in rainfall in the last decade, overexploitation of groundwater, the construction of dams, the development of tourism, and the increase in the area under rice cultivation. This has led to the salinity of the soil and groundwater, as well as seawater intrusion (Golshan et al. 2018; Sahour et al. 2020). Considering the strong dependence of agricultural lands and urban areas of this region on groundwater, it is important to evaluate the spatiotemporal changes of salinity and its causative factors.

Reviewing previous studies, like Gholami et al. (2009), Moghimi et al. (2016), Motevalli et al. (2018), Nezhadnaderi (2018), Golshan et al. (2018), Janardhana and Khairy (2019), Moghimi (2017), Khairy and Janardhana (2021), Sahour et al. (2020), and Mazandaran regional water company (MRWC) reports, reveals that in the four-layer aquifer of the GH.-J. study area, a precise and specific study has not been done to determine the factors that cause salinity separately in all of the aquifers of this plain. In these studies, research has mainly been focused on the modeling of the western aquifers of the Caspian coastal strip and their hydrogeochemical investigation as a result of agricultural land

development. Therefore, the development of an integrated approach of statistical tools and hydrogeochemical analyses using GIS to evaluate SWI in GH.-J. aquifer is proposed as a new research, and it is necessary to fill the existing research gaps in this field. Also, the identification of locations contaminated with salinity and susceptible to SWI for each of the four layers of the aquifer, along with determining their origin, is considered a new and innovative achievement. Furthermore, the results of this study not only raise awareness among farmers but they can also play a significant role in the proper management of land, promoting the adoption of sustainable policies in the operation of coastal aquifers. Due to the proximity of the studied aquifer to the Caspian Sea and its presence with multiple layers, this research investigated the behavioral changes in hydrogeochemical characteristics of the aquifer. This exploration aimed to identify the source of saltwater intrusion and understand the reasons behind its increase over a long-term period (2011–2020). To achieve this objective, we utilized a combination of results from statistical methods and principal components analysis, along with modified Piper diagram indexes ($GQI_{\text{Piper(mix)}}$ and $GQI_{\text{Piper(dom)}}$), the intrusion of saltwater in coastal aquifers index (GQI_{SWI}) (Tomaszkiewicz et al. 2014), and HFE-D (Gimenez-Forcada 2010; 2014). Additionally, we employed the GIS technique, which had not been previously considered in the study area. Based on the proposed approach, the salinity status and qualitative changes of the aquifer due to the effects of SWI and other geogenic or anthropogenic factors affecting it during a 10-year period were investigated by comparing and evaluating the methods mentioned above. The results of the applied methods were presented using the GIS technique in the form of spatiotemporal distribution of the aquifer freshening and intrusion phases. Therefore, the most important goals of the present study are:

- Identifying and distinguishing between various factors contributing to the salinity of aquifers in the studied area, based on the dominant qualitative type, ion ratios, correlation status, and principal component analysis
- Spatiotemporal investigation of changes in concentration of major ions related to geochemical evolution during saltwater intrusion process using GQI_{SWI} index, modified Piper diagram, and HFE-D.
- Determining natural (geogenic) and artificial (anthropogenic) sources of salinity in different layers of the aquifer

The findings of the present research can offer a clear insight into understanding the origin and governing mechanisms of salinity in this multilayered coastal aquifer. Additionally, based on these findings, it is possible to formulate and develop operational instructions for the coastal aquifer, aiming to achieve a qualitative revival for sustainable harvesting.
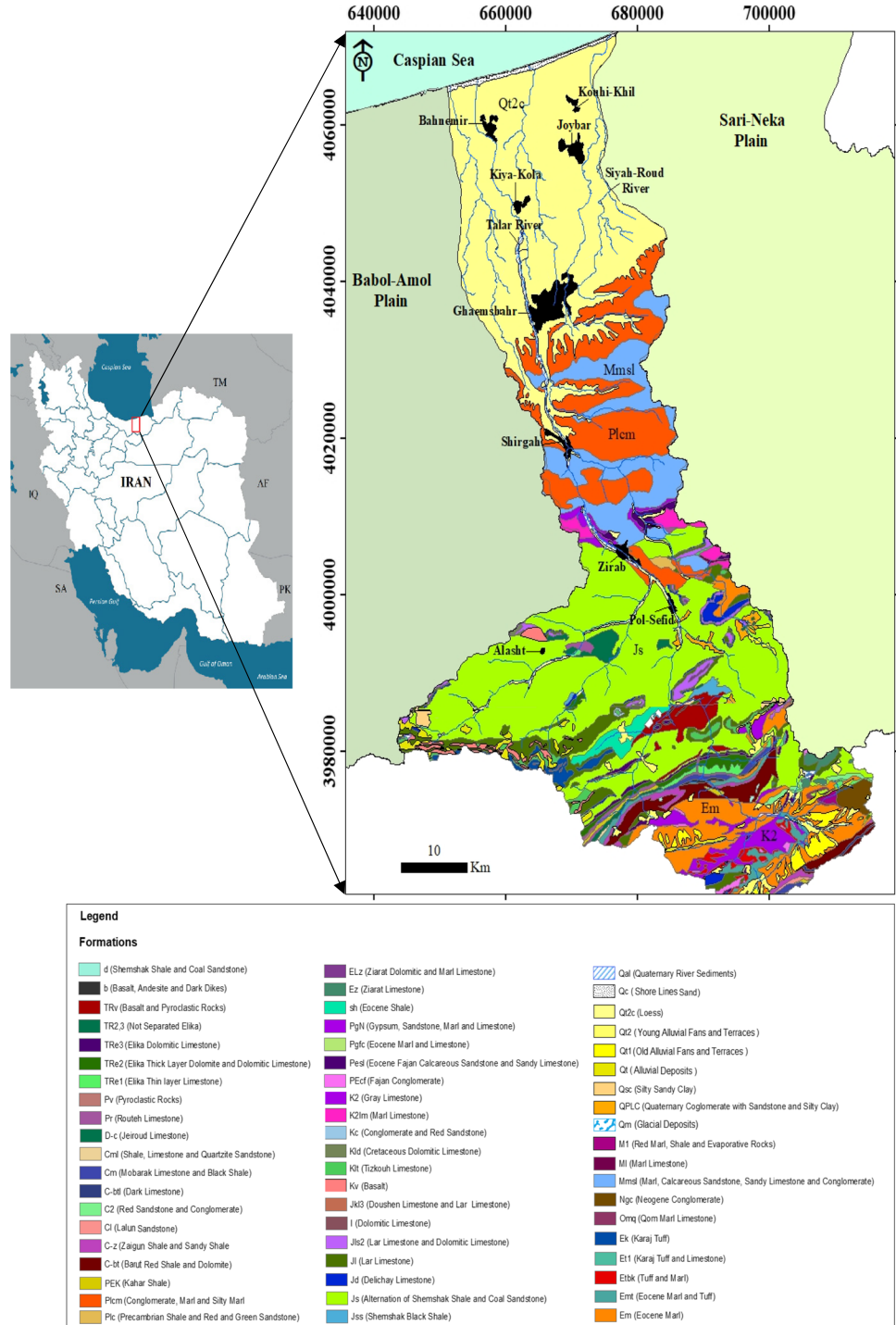
Materials and methods

Description of the study area

The studied area of GH.-J. is an example of a coastal aquifer at risk of saltwater intrusion, which is located in the coastal belt of the Caspian Sea. This aquifer is located in the north of Iran and between the two aquifers of Sari-Neka in the east and Babol-Amal in the west. The total area of the study area is about 3537 km^2, of which 935.5 km^2 is plain. The rest is the heights of the northern slopes of the Alborz Mountains (Fig. 1). The highest and lowest altitude of the this plain are 3929 and −26 msl (mean sea level), respectively (Mazandaran Regional Water Organization 2010).

Fig. 1 Geological map of the study area

Legend

Formations

d (Shemshak Shale and Coal Sandstone)	ELz (Ziarat Dolomitic and Marl Limestone)	Qal (Quaternary River Sediments)
b (Basalt, Andesite and Dark Dikes)	Ez (Ziarat Limestone)	Qc (Shore Lines Sand)
TRv (Basalt and Pyroclastic Rocks)	sh (Eocene Shale)	Qt2c (Loess)
TR2,3 (Not Separated Elika)	PgN (Gypsum, Sandstone, Marl and Limestone)	Qt2 (Young Alluvial Fans and Terraces)
TRe3 (Elika Dolomitic Limestone)	Pgfc (Eocene Marl and Limestone)	Qt1 (Old Alluvial Fans and Terraces)
TRe2 (Elika Thick Layer Dolomite and Dolomitic Limestone)	Pesl (Eocene Fajan Calcareous Sandstone and Sandy Limestone)	Qt (Alluvial Deposits)
TRe1 (Elika Thin layer Limestone)	PEcf (Fajan Conglomerate)	Qsc (Silty Sandy Clay)
Pv (Pyroclastic Rocks)	K2 (Gray Limestone)	QPLC (Quaternary Coglomerate with Sandstone and Silty Clay)
Pr (Routeh Limestone)	K2lm (Marl Limestone)	Qm (Glacial Deposits)
D-c (Jeiroud Limestone)	Kc (Conglomerate and Red Sandstone)	M1 (Red Marl, Shale and Evaporative Rocks)
Cml (Shale, Limestone and Quartzite Sandstone)	Kld (Cretaceous Dolomitic Limestone)	Ml (Marl Limestone)
Cm (Mobarak Limestone and Black Shale)	Klt (Tizkouh Limestone)	Mmsl (Marl, Calcareous Sandstone, Sandy Limestone and Conglomerate)
C-btl (Dark Limestone)	Kv (Basalt)	Ngc (Neogene Conglomerate)
C2 (Red Sandstone and Conglomerate)	Jkl3 (Doushen Limestone and Lar Limestone)	Omq (Qorm Marl Limestone)
Cl (Lalun Sandstone)	I (Dolomitic Limestone)	Ek (Karaj Tuff)
C-z (Zaigun Shale and Sandy Shale)	Jls2 (Lar Limestone and Dolomitic Limestone)	Et1 (Karaj Tuff and Limestone)
C-bt (Barut Red Shale and Dolomite)	Jl (Lar Limestone)	Etbk (Tuff and Marl)
PEK (Kahar Shale)	Jd (Delichay Limestone)	Emt (Eocene Marl and Tuff)
Plcm (Conglomerate, Marl and Silty Marl	Js (Alternation of Shemshak Shale and Coal Sandstone)	Em (Eocene Marl)
Plc (Precambrian Shale and Red and Green Sandstone)	Jss (Shemshak Black Shale)	

Considering the importance of this region in the production of agricultural products (especially citrus fruits and rice), it is necessary and worthy of attention to investigate the changes and reasons for the qualitative degradation of the groundwater resources of this plain. The coastal alluvial sediments of the studied area have created a multilayered aquifer system.

The highest layer is the unconfined aquifer, used for agriculture, drinking, industry, and aquaculture (fish farming) purposes. This layer has formed a perched aquifer in parts of the margin of the Caspian Sea due to the placement of fine-grained clay layers under it, which has good quality for drinking and agricultural purposes.

In the distance between the perched and unconfined, fossil saline waters are trapped in the alluvial layer and have formed a low-quality saline aquifer. The lowest layer is located in the southern part of the plain, which, due to being under the marl and clay impermeable layer, has formed a confined aquifer with good quality for agricultural and drinking purposes.

The 10-year average amount of annual precipitation in the studied plain is equal to 696.2 mm. The highest and lowest monthly precipitation occurs in November and June, with values of 216.7 and 0.3 mm, respectively. Based on the average data of 25 years, the amount of annual evaporation in the plain is 1060.34 mm, and the minimum and maximum temperature reported in the plain is for January and August with values of 7 °C and 25 °C, respectively. The climate of the study area is considered to be moderate to very humid based on the Emberger climate classifications (Mazandaran Regional Water Organization 2010).

Geologic and hydrogeologic units

In the study area, there are various geological formations from the early carboniferous to the quaternary (Fig. 1). One-third of the heights is occupied by the Shamshak formation (sandstone, quartz sandstone, coal shales, and clay rocks), which has a quantitative and qualitative relationship with the plain aquifer due to the presence of numerous faults. The carbonate formations of Elika (shale and dolomitic limestone), Delichai (calcareous marl and marl limestone), and Lar (limestone and dolomitic limestone) have the most significant impact on the quality of the groundwater in terms of solubility.

Cretaceous Tizkoh formation (dolomite limestone, limestone with volcanic rocks) is observed on the border of mountains and plains. By moving towards the plain, quaternary sediments, including the Apsheron Formation (Lower quaternary), can be seen, which are formed from stiff clays, marl, sand, gravel layers, and a thin layer of volcanic ash in lake conditions. The water left over from the retreat of the Caspian Sea in different geological periods on Apsheron

sediments and then covering these waters with new Caspian sediments has caused the formation of fossil saline aquifers. Apsheron formation is covered with lacustrine sediments, including sand, unhardened mud (New Caspian), and discontinuous sediments, which created the unconfined aquifer with relatively good permeability of GH.-J. plain (Fig. 1). In fact, the type of bedrock has not been determined in the studied area. The structure of the alluvial unconfined aquifer is formed from river alluvium and lake sediments containing freshwater, which are placed on fossil saltwater. Accordingly, the lower layer of this aquifer is formed by the saltwater arch.

In the southern part of the plain, due to the presence of clay and marl layers, a confined aquifer is formed under the unconfined aquifer. The expansion of saline aquifers or aquifers with poor quality has also been identified based on the groundwater qualitative data in the northern part of the plain.

The alluvium in the north of the GH.-J. plain and on the margin of the Caspian Sea is finer-grained with clay, forming the perched aquifer in this part. Therefore, in the studied area, four aquifers (perched, saline, unconfined, and confined) have been created, and the boundaries of these aquifers are shown in Fig. 2. In the GH.-J. plain, the alluvium in the surface parts of southern areas is fine-grained and becomes coarser in the depths (Fig. 3). Also, the greatest thickness of the aquifer has been identified in the middle part of the plain. The area of unconfined and confined aquifers is 614.24 and 376.13 km^2, respectively. The potential of the water withdrawal from groundwater in this plain is approximately 343,000 m^3/year/km^2 (Geological Survey of Iran 2003). In the study area, due to the low number of exploration wells, inappropriate dispersion in the plain, and limited geophysical information, it is not possible to accurately estimate the exact hydrogeological sections, the depth of discontinuous sediments, and the exact surface of the salt–freshwater interface. Figure 4 shows the schematic hydrogeological cross section of GH.-J. plain based on available geological information and exploration logs (Fig. 3) along the line from south to north (from Alborz mountain to Caspian Sea).

Water sampling and analyses

By early 2000, in the studied area, the number of observation wells and hydrochemical data in the aquifers in order to the quality situation monitoring was very few and limited. During 2000–2010, the quality monitoring wells in the unconfined aquifer increased somewhat, but the data related to the quality status of other aquifers was sporadically collected. In fact, during this period, sufficient data were not available in terms of the number and measurement of quality parameters to evaluate the quality of aquifers. Since 2010, with the
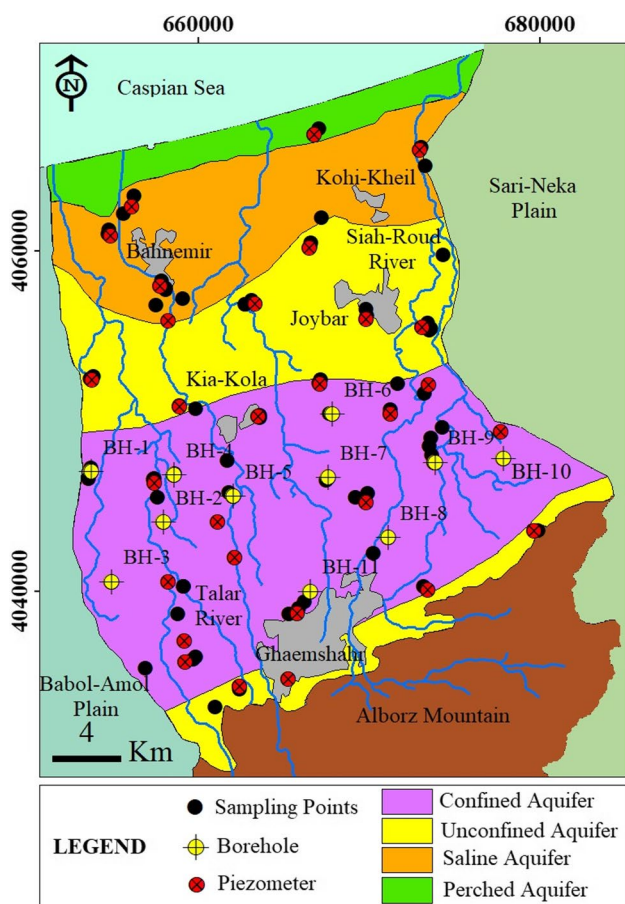
Fig. 2 Location of the sampling points, piezometers, boreholes, and all of the aquifers located in the GH.-J. plain

increase in observation wells and regular sampling, a complete set of hydrochemical data was provided for the qualitative study of the plain and coastal aquifer management. In this study, the 49, 31, 30, and 30 samples from semi-deep wells of unconfined aquifer; 22, 15, 12, and 13 samples from deep wells of confined aquifer; and 13, 5, 2, and 5 samples from saline aquifer were collected during 2011, 2014, 2017, and 2020, respectively. Also, two samples were taken from the perched aquifer every 4 years. In early 2013, the number of wells was limited, and the hydrochemical data were incomplete. The decrease in the number of samples during different years is due to the drying up of some wells due to the excessive exploitation in recent years, making some of the wells unavailable.

Samples were collected by Mazandaran Regional Water Company, and their chemical analyses were performed according to American Public Health Association (APHA 2005) standards by the laboratory affiliated with this company. In this research, purging and sampling wells without plumbing, within the limit of suction, were done by the bailer. Before sampling, the purging process involved using

a bailer conforming to the Standard Operating Procedure for Field Equipment Cleaning and Decontamination (SES-DPROC-205). A closed-top Teflon bailer with Teflon-coated stainless steel leaders and a new nylon rope was lowered into the top of the water column, filled, and withdrawn, removing stagnant water from the well just before sampling. This process ensured its replacement by groundwater from the adjacent formation, representing actual aquifer conditions. It is critical that the bailer must be slowly and gently immersed into the top of the water column, particularly during the final stages of purging, to minimize turbidity and disturbance of volatile organic constituents. In this method, a bailer was used to purge and sample the wells, and a new bailer rope was not required between purging and sampling (Puls and Barcelona 1996). After purging, the bailer was gently immersed in the top of the water column until it was just filled. At this point, the bailer was slowly removed, and the contents were emptied into the appropriate sample containers (250-ml polyethylene bottles).

Temperature, pH, and EC parameters were measured in situ using the HACH Multimeter device (HACH, Germany). The collected samples were placed in an ice box and transferred to the water laboratory of Mazandaran Regional Water Company, Iran, in a short time and stored at 4 °C in the refrigerator for analysis. The concentrations of the main ions in this laboratory were analyzed employing APHA standard methods (APHA 2005): sodium and potassium using flame photometry, calcium, and magnesium by titration method with EDTA, alkalinity (HCO_3) by volumetric titration with HCL and methyl orange, chloride by standard $AgNO_3$ titrations, and sulfate by the measured by $BaCl_2$ method using spectrophotometer.

Charge balance error (CBE) was used to evaluate the accuracy of the measured data (Asare et al. 2021; Chitsazan et al. 2017). Calculating the value of this index for all samples shows that the error rate is less than $\pm 5\%$, and therefore, the qualitative data have good accuracy for subsequent analyses.

The background of the used theoretical methods

Statistical techniques

In general, understanding hydrological and geochemical processes in coastal aquifers is very difficult due to their complexity. So, descriptive statistical methods can be very effective and helpful in analyzing complex hydrochemical processes in the groundwater by using hydrochemical data and correlation matrix analysis (CMA) between two or more variables. It should be noted that correlation analysis plays an important role in determining the origin of ions in groundwater sources (Islam et al. 2017; Li et al. 2020; Su et al. 2017).
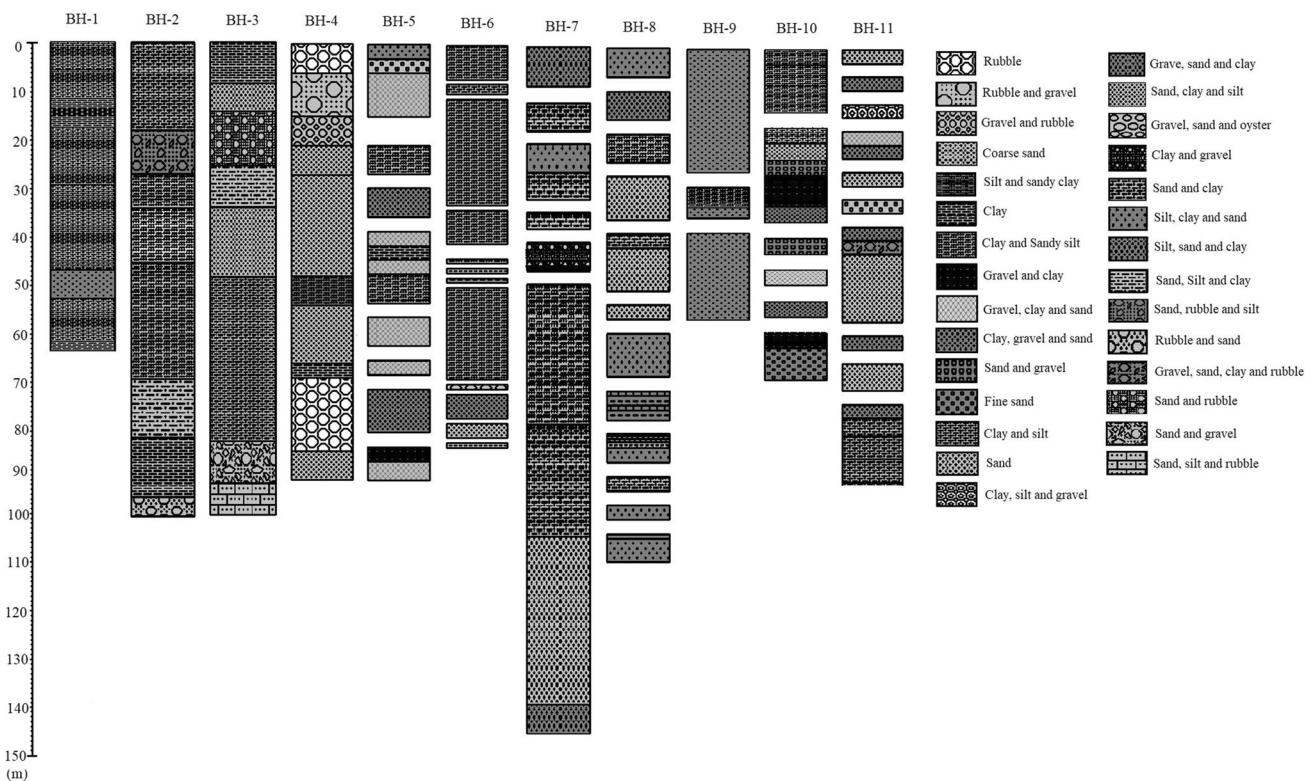
Fig. 3 Logs of boreholes located in the central part of GH.-J. plain
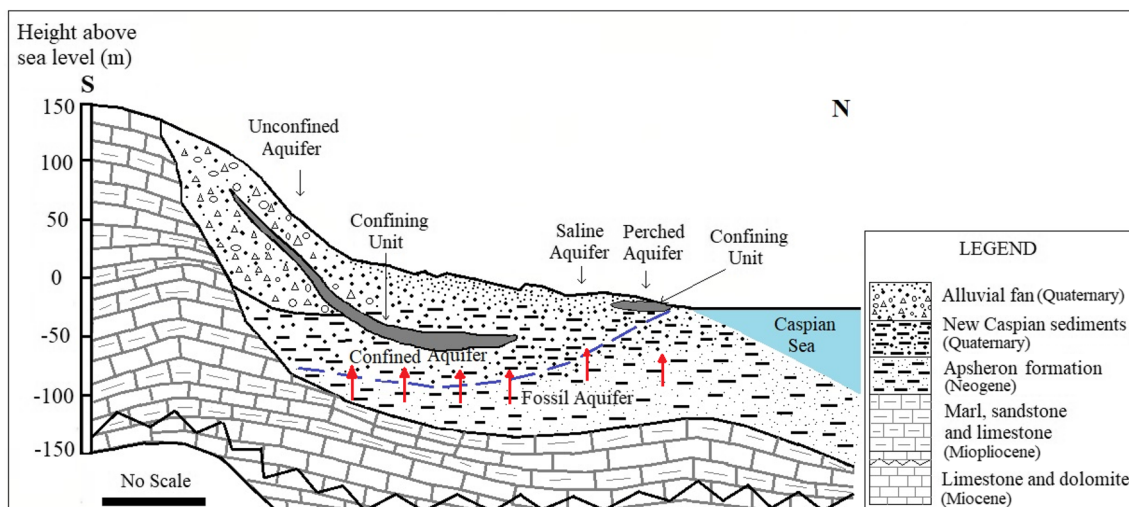

Fig. 4 Schematic hydrogeological cross section along line S–N in the GH.-J. plain. The blue line denotes the hypothetical separation surface of fresh and saline groundwater, and the red arrows show saline groundwater flow directions from the fossil aquifers to the unconfined and confined aquifers

Multivariate statistical methods are instrumental in obtaining significant information from hydrogeochemical data sets of aquifers and have good efficiency. In this study, principal component analysis (PCA) was applied to determine the relationships between variables in order to evaluate the processes that control water chemistry. So far, this method has been used by many researchers in hydrochemical research (Elemile et al. 2021; Mohammed Siraj Ansari and Saraswathi 2022; Nemati et al. 2022; Nguyen et al. 2020).

To identify the hydrogeochemical processes in coastal aquifers and determine the origin of important anions and cations in them, hydrogeochemical data are grouped using the PCA approach and according to the qualitative characteristics inherited from the groundwater or saltwater. The main goal of this method is to reduce the contribution of less significant variables to further simplify the data structure. This method begins by coding all variables with a mean of zero and a variance of one and finding the corresponding eigenvalues and eigenvectors. Then, the data is converted into components. Kaiser (1958) used the minimum acceptable eigenvalue of 1 as a criterion to determine the number of components (PCs). In this research, the extraction of components was done with the same criterion for the total number of samples (Mahlknecht et al. 2004). In this study, all the statistical analyses were performed using the Excel 2019 and IBM Statistic SPSS 26 software. Additional explanations related to the CMA and PCA are provided in part I of supplementary information.

Piper diagram and saltwater intrusion groundwater quality index (GQI$_{SWI}$)

Hydrogeochemical concepts, utilizing environmental data and drawing them in the form of a single diagram, can help describe and understand the mechanisms of flow and transport of materials in groundwater systems. One of the widely used and handy diagrams for producing and determining the relationships between the concentration of different ions dissolved in water and classifying water based on their chemical properties is the Piper diagram. The Piper diagram allows for the determination of hydrogeochemical facies of water by assessing the relative characteristics of dominant ions in the collected samples (Amiri et al. 2015; Mohammadi Arasteh and Shoaei 2020; Piper 1944; Sarath Prasanth et al. 2012; Subramani et al. 2005).

This diagram consists of triangles of the main anions and cations, each side of which is divided linearly from 0 to 100. By placing the qualitative parameters related to the measured samples on this graph and determining their position, the state of sea saltwater intrusion, the possibility of salt and freshwater mixing, and the groundwater hydrochemical facies are determined. In this diagram, six regions representing different types of water can be identified (Fig. 5) (Amiri et al. 2015; Sarath Prasanth et al. 2012; Subramani et al. 2005). More details of the Piper diagram are described in part I of supplementary information.

In order to determine the amount of seawater intrusion, *GQI*$_{flake}$ index was proposed by Appelo and Postma (2004) using the theoretical mixing percentage and considering chloride as a conservative ion (Eq. 2). This index is based on Tomaszkiewicz et al. (2014) due to its high sensitivity to the chlorine parameter; it cannot independently
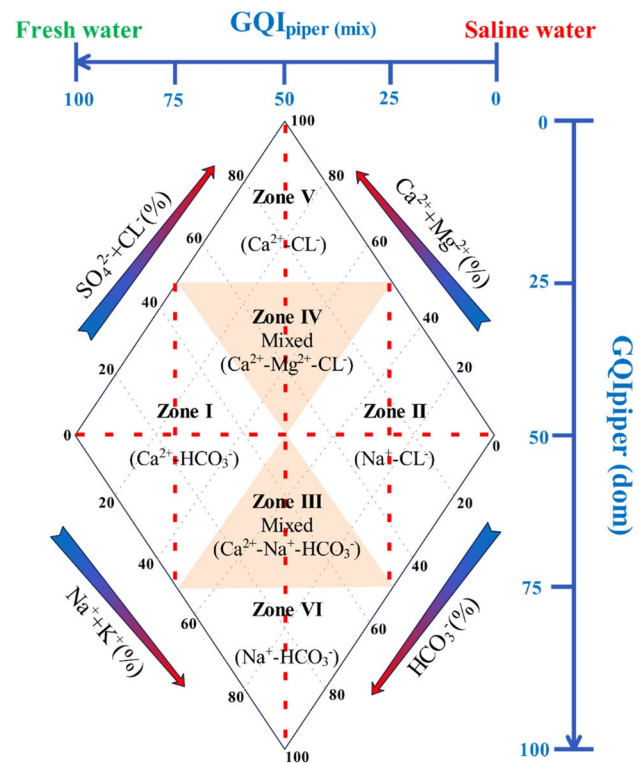

Fig. 5 Description of created Piper domains based on *GQI*$_{Piper(mix)}$ and *GQI*$_{Piper(dom)}$ indexes (redesign based on Tomaszkiewicz et al. (2014))

detect the dominant hydrogeochemical reactions in the phenomenon of seawater intrusion and has weaknesses. Based on this, they proposed a combination of *GQI*$_{flake}$ and *GQI*$_{Piper(mix)}$ under the title of *GQI*$_{SWI}$ index (Eq. 3). This index shows a more representative index for seawater mixing by using the strengths of two combined indices and compensating for their weaknesses.

$$f_{lake} = \frac{C_{Cl,sample} - C_{Cl,fresh}}{C_{Cl,lake} - C_{Cl,fresh}} \times 100 \tag{1}$$

$$GQI_{flake} = (1 - f_{lake}) \times 100 \tag{2}$$

$$GQI_{SWI} = \frac{GQI_{Piper(mix)} + GQI_{flake}}{2} \tag{3}$$

where $C_{Cl,sample}$ and $C_{Cl,fresh}$ are the chloride concentrations in the sample and Caspian Sea (6500mg/l), respectively (Table 1). The $C_{Cl,fresh}$ is the chloride concentration in the groundwater.

The status of the water type in terms of salt and freshwater mixing based on the *GQI*$_{SWI}$ index is as follows:

$$0 < GQI_{SWI} < 10: \text{freshwater}$$

Table 1 Mean concentration of solution elements in oceans and seas (Hem 1970) and Caspian Sea (Ministry of Jihad-e-Agriculture 2006)

Chemical parameters (g/l)	Cl^-	Na^+	SO_4^{2-}	Mg^+	Ca^{2+}	K^+	HCO_3^-	TDS	EC (mS/cm)
Oceans and seas	19	10.5	2.7	1.35	0.41	30.9	0.142	35	55
Caspian sea (ave.)	6.5	3.1	3.6	1.1	0.45	0.08	1	12.6	20

$10 < GQI_{SWI} < 50$: mixed groundwater
$50 < GQI_{SWI} < 75$: saline groundwater
$75 < GQI_{SWI} < 100$: seawater

Hydro-chemical facies evolution diagram (HFE-D) to assess the evolution of seawater intrusion and freshening stages

The chemical composition of aquifers qualitatively changes along its flow path from recharge areas to a discharge point. This change results from the long interaction of water and rock, evapotranspiration, and the effects of seawater. Therefore, in a closed system, the hydrochemical changes of the main ions can indicate the gradual expansion of pollutants in the regional flow system (Asare et al. 2021). In coastal aquifers affected by seawater intrusion, a sequence of geochemical reactions occur when freshwater is replaced by seawater. These chemical changes can be attributed to variations in the chemical characteristics of the recharge source, aquifer constituents, and fluctuations in groundwater level. Based on the literature review, the HFE-D can present the process

of these changes much more useful than the Piper diagram method (Hajji et al. 2021; Le et al. 2020).

This diagram, which was first proposed by Gimenez-Forcada (2010), is a simple and robust method to identify the condition of coastal aquifers exposed to seawater intrusion, the percentage of salt and freshwater mixing, and checking the interference positions of sea saltwater using the distribution of anion and cation percentages in the form of a specific diagram (Giménez-Forcada and Sánchez San Román 2015). During the process of sea saltwater intrusion (intrusion stage), the aquifer is affected by two simultaneous processes: salinity increase due to the rapid exchange of Na^+ with Ca^{2+} and reverse exchange reactions (lines II and VI in Fig. 6). As a result of these processes, the Ca–Cl facies is developed. After that, the qualitative composition of the groundwater becomes $Na^+ - CL^-$ facies due to the movement towards the salty seawater (line III in Fig. 6). In other words, when a saltwater intrusion occurs in coastal aquifers, hydrochemical facies change from $Ca^{2+} - HCO_3^-$ to $Ca^{2+} - CL^-$ and finally to $Na^+ - CL^-$.

Fig. 6 Hydrochemical facies evolution diagram (HFE-D) (redesign based on Amiri et al. (2015); Le et al. (2020))

Zone 1: Na-HCO₃/SO₄
Zone 4: Na-Cl
Zone 7: MixNa-MixCl
Zone 10: MixCa-MixHCO₃/MixSO₄
Zone 13: Ca/Mg-HCO₃/SO₄
Zone 16: Ca/Mg-Cl

Zone 2: Na-MixHCO₃/MixSO₄
Zone 5: MixNa-HCO₃/SO₄
Zone 8: MixNa-Cl
Zone 11: MixCa-MixCl
Zone 14: Ca/Mg-MixHCO₃/MixSO₄

Zone 3: Na-MixCl
Zone 6: MixNa-MixHCO₃/MixSO₄
Zone 9: MixCa-HCO₃/SO₄
Zone 12: MixCa-Cl
Zone 15: Ca/Mg-MixCl
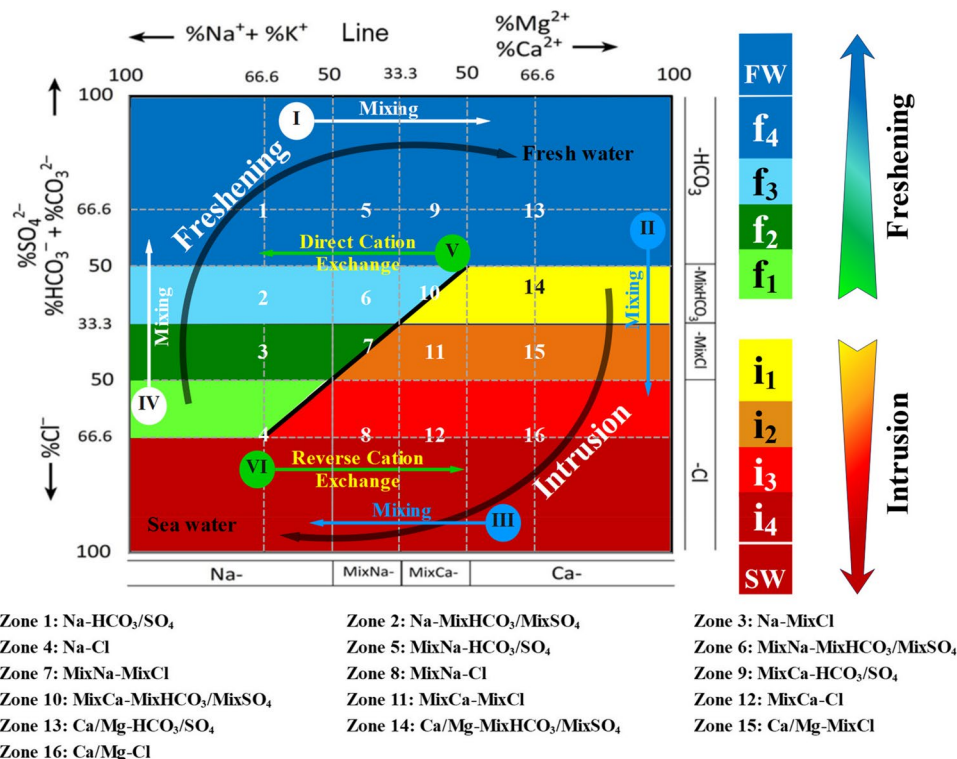
During the freshening process, freshwater recharge leads to direct exchange reactions (lines V and IV in Fig. 6) and the formation of $Na^+ - HCO_3^-$ facies. Finally, the water becomes freshwater due to mixing with the aquifer (line I) (Amiri et al. 2015; Gimenez-Forcada 2010). Accordingly, when freshwater feeding is dominant in coastal aquifers, Na^+ replaces Ca^{2+}, and the hydrochemical facies change from $Na^+ - CL^-$ to $Na^+ - HCO_3^-$.

According to the above explanations and based on the percentage of main ions (sum of sodium and potassium, calcium, bicarbonate, and chloride), the qualitative samples of the aquifer can be divided into 16 hydrochemical facies, and if magnesium and sulfate are also considered, the number of hydrochemical facies increases to 32. If the percentage of calculated ions is greater than 50%, four main facies can be identified in the HFE-D diagram, which is as follows: $Na^+ - HCO_3^-$ (saltwater under the influence of direct cation exchanges), $Na^+ - Cl^-$ (seawater), $Ca^{2+} - HCO_3^-$ (freshwater), and $Ca^{2+} - Cl^-$ (Saltwater under the influence of reverse cation exchange). If the the calculated percentage for some of the mentioned anions and cations is less than 50%, while simultaneously exceeding 50% for others, the facies are identified with the mix prefix (Le et al. 2020).

On the HFE-D diagram, the line that separates the saltwater and freshwater of the aquifer is considered the conservative mixing line (CML). Its position is determined by analyzing the chemical composition of samples taken from the aquifer (Gimenez-Forcada 2010).

The two arrows around the CML line represent the evolutionary reactions of water hydrogeochemical changes during intrusion (reverse exchange reactions) and freshening (direct exchange reactions). The sediments in the groundwater aquifers of the study area have a mixed marine-alluvial origin, characterized by interlayers of clay, silt, sand, and coarse to fine sand. (Mazandaran Regional Water Organization 2010). Clay minerals in sediments provide suitable chemical conditions for direct and reverse cation exchanges.

To closely examine the governing processes during the freshening and intrusion stages on the HFE-D diagram, these stages are subdivided into sub-stages that illustrate the spread of salinity based on the percentage of ions. With this information, the sub-stages marked with "i" and "f" represent the intrusion and freshening stages, respectively (Giménez-Forcada 2019).

In this study, in order to show the spatial distribution of dominant facies in the intrusion and freshening processes, each of the sub-stages was given a score from 1 to 10. In this scoring, the minimum and maximum assigned to freshwater (FW) and seawater (SW) are equal to 1 and 10, respectively. Also, for sub-stages f_4, f_3, f_2, and f_1, scores in the range of 2 to 5, and for sub-stage i_1, i_2, i_3, and i_4, scores from 6 to 9 were considered. According to the coloring of each of the sub-stages and extracting the spatial distribution of different water types using ArcGIS 10.8, it becomes possible to identify each of the sub-stages related to the intrusion and freshening processes (Table 2). The stages for assessing

Table 2 Values and colors considered to identify miscellaneous hydrochemical facies based on Giménez-Forcada (2014) and Le et al. (2020) studies

Domain	Substage	Zone	Water Type	Value	Range of variation	Color
Intrusion phase	SW	4	Na-Cl	10	≥8.5	
	i_4	16,12,8,4	Ca-Cl, MixCa-Cl, MixNa-Cl (%Cl>66.6)	9		
	i_3	16,12,8, part of 4	MixNa-Cl (50<%Cl<66.6), MixCa-Cl, Ca-Cl	8	7.6-8.5	
	i_2	15, 11, half of 7	MixNa-MixCl, MixCa-MixCl, Ca-MixCl	7	6.6-7.5	
	i_1	14, half of 10	MixCa- MixHCO$_3$, Ca-MixHCO$_3$	6	5.6-6.5	
Freshening phase	f_1	Part of 4	Na-Cl (50<%Cl<66.6)	5	4.6-5.5	
	f_2	3, half of 7	Na-MixCl, MixNa-MixCl	4	3.6-4.5	
	f_3	2,6, half of 10	Na-MixHCO$_3$, MixNa-MixHCO$_3$, MixCa-MixHCO$_3$	3	2.6-3.5	
	f_4	1,5,9,13	Na-HCO$_3$, MixNa-HCO$_3$, MixCa-HCO$_3$, Ca-HCO$_3$ (Ca<66.6)	2	≤2.5	
	FW	13	Ca-HCO$_3$	1		

potential seawater intrusion in the GH.-J. multilayered aquifer, as described above, are presented in Fig. 7.

Results and discussion

Chemical composition of groundwater samples of the coastal multilayered aquifer of GH.-J.

Analyzing qualitative samples drawn between 2011 and 2020 on the modified Piper diagram (Fig. 13) reveals that the predominant water type in the unconfined aquifer is mixed Ca–Mg–Cl and Ca–HCO$_3$; in the saline aquifer, it is mixed Ca–Mg–Cl; in the perched aquifer, it is Ca–HCO$_3$; and in the confined aquifer, it is mixed Ca–Mg–Cl and Ca–HCO$_3$. Furthermore, significant changes have been observed in the chemical composition and salinity of groundwater samples across various layers of the studied aquifers.

The range of variations of the main cations and anions, as well as the minimum and maximum values of TDS (mg/l) and EC (μs/cm) of four aquifers during a 10-year period, is according to Table 3. In most areas, a TDS value greater than 1000 mg/l typically indicates salinity, except in dry regions where water scarcity is prevalent, and low-quality water is commonly utilized. (Elgettafi et al. 2012). The pH value of all aquifers is in the neutral range between 6 and 8. The dominant cations and anions of the groundwater in the four aquifers are Ca^{2+}, Na$^+$, HCO$_3^-$, and Cl$^-$. Overall, in the studied area, the concentration of Ca^{2+} cation in unconfined, confined, and perched aquifers exceeds

that of Na$^+$, except in the saline aquifer, the concentration of Na$^+$ surpasses that of Ca^{2+} in the years 2011 and 2017. The concentration of NO$_3^-$ in the years 2014 and 2020 significantly increases in many wells across all aquifers. This suggests that the pollution is local and temporary and is caused by the elevated use of nitrogen-containing urea fertilizer in agricultural farms for rice cultivation.

To explore the reasons for changes in the concentration of various ions and investigate the sources of their release in groundwater, creating scatter plots of different ions versus chloride ions, as well as examining the ratio of different ion pairs and saturation index, can offer valuable insights into the origin of salinity and its intrusion (Figs. 1, 2, 3, 4, 5, 6 and 7, along with Fig. 8, are presented in part II of Supplementary information).

- Based on the scatter plots drawn between anions and cations relative to the stable ion Cl$^-$, it can be seen that Cl$^-$ has a strong positive correlation with TDS, EC, and Na$^+$. Therefore, this ion is the controller of EC in the studied coastal aquifer (Carol and Kruse 2012). Also, chloride ion shows a weak positive correlation with Ca^{2+}, Mg^{2+}, NO$_3^-$, HCO$_3^-$, and SO$_4^{2-}$. The correlation of Mg^{2+} ion with Na$^+$, K$^+$, and Ca^{2+} is positive but not strong. This is attributed to the influence of other sources, in addition to sea saltwater intrusion, contributing to the increased salinity of the aquifer. (Asare et al. 2021).
- A TDS versus EC plot showing a slope above 0.99, significantly exceeding the range of 0.55–0.75 reported by

Table 3 The decreasing order of major cations and anions in unconfined, confined, saline, and perched aquifers in 2011, 2014, 2017, and 2020 years

| Aquifer type	Year			
	2011	2014	2017	2020
Unconfined	Cations	Ca > Na > Mg > > K	Ca > Na > Mg > > K	Ca > Na > Mg > > K	Ca > Na > Mg > > K
	Anions	HCO$_3$ > Cl > NO$_3$ > SO$_4$	NO$_3$ > HCO$_3$ > Cl > SO$_4$	HCO$_3$ > Cl > SO$_4$ > NO$_3$	NO$_3$ > HCO$_3$ > Cl > SO$_4$
	TDS (mg/l)	(461–2398)	(500–1788)	(586–2110)	(523–1735)
	EC (μs/cm)	(710–3580)	(770–2670)	(904–3145)	(805–2590)
Confined	Cations	Ca > Na > Mg > > K	Ca > Na > Mg > > K	Ca > Na > Mg > > K	Ca > Na > Mg > > K
	Anions	HCO$_3$ > Cl > NO$_3$ > SO$_4$	NO$_3$ > HCO$_3$ > Cl > SO$_4$	HCO$_3$ > Cl > SO$_4$ > NO$_3$	NO$_3$ > HCO$_3$ > Cl > SO$_4$
	TDS (mg/l)	(222–1829)	(383–1194)	(415–1341)	(138–1488)
	EC (μs/cm)	(347–2730)	(596–1790)	(621–2001)	(220–2220)
Saline	Cations	Na > Ca > Mg > > K	Ca > Na > Mg > > K	Na > Ca > Mg > > K	Ca > Na > Mg > > K
	Anions	Cl > HCO$_3$ > SO$_4$ > NO$_3$	NO$_3$ > HCO$_3$ > Cl > SO$_4$	HCO$_3$ > Cl > SO$_4$ > NO$_3$	NO$_3$ > HCO$_3$ > Cl > SO$_4$
	TDS (mg/l)	(568–4448)	(860–1845)	(646–1430)	(574–1514)
	EC (μs/cm)	(874–6640)	(1311–2755)	(995–2140)	(883–2260)
Perched	Cations	Ca > Na > Mg > > K	Na > Ca > Mg > > K	Ca > Na > Mg > > K	Ca > Mg > Na > > K
	Anions	NO$_3$ > SO4 > Cl > HCO$_3$	NO$_3$ > HCO$_3$ > Cl > SO$_4$	HCO$_3$ > Cl > SO$_4$ > NO$_3$	NO$_3$ > HCO$_3$ > SO$_4$ > Cl
	TDS (mg/l)	(1146–1310)	(859–1129)	(652–856)	(448–636)
	EC (μs/cm)	(1737–1956)	(1311–1698)	(1004–1306)	(695–979)
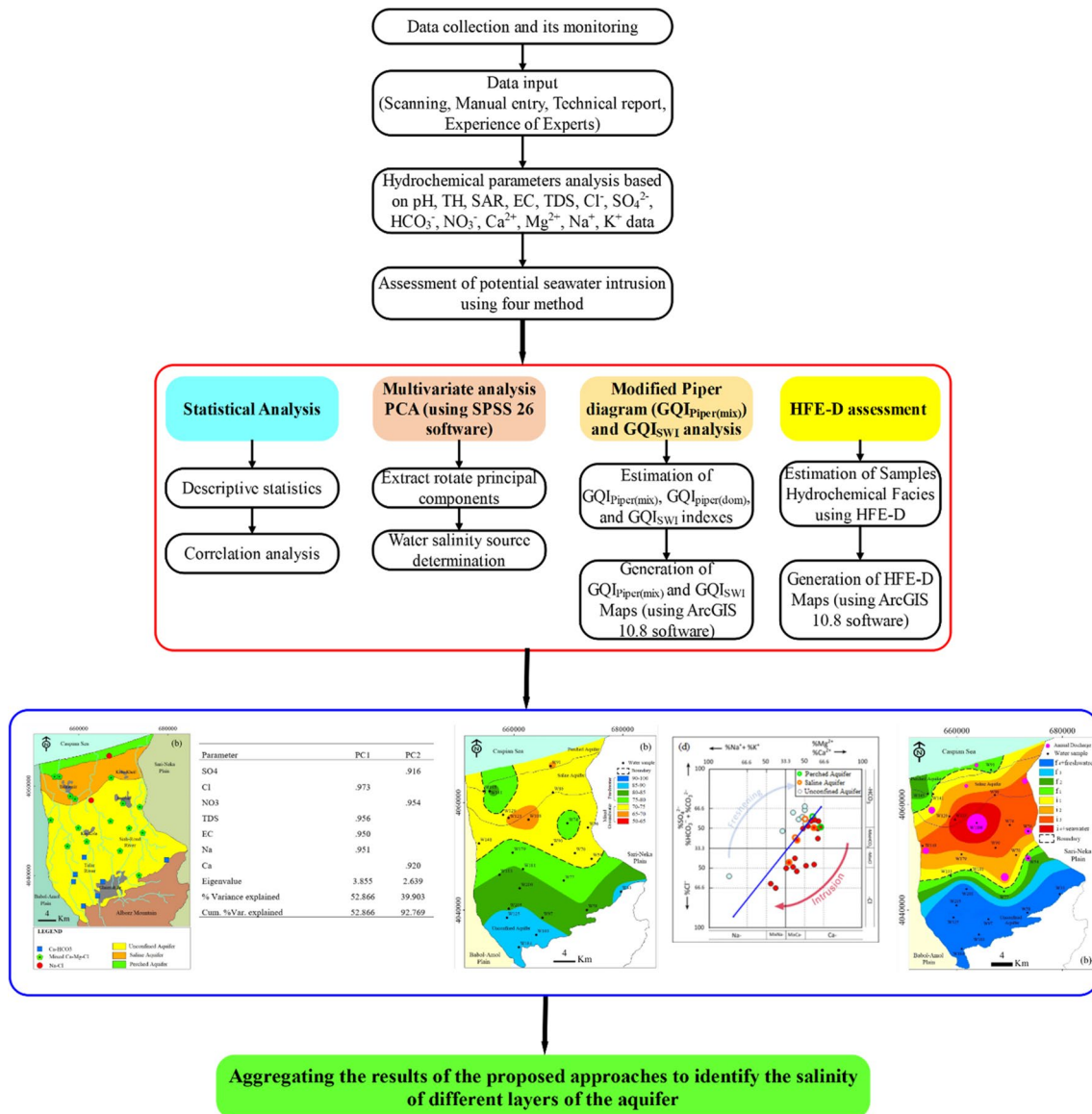
Fig. 7 Flowchart of proposed methodology to assess potential seawater intrusion

Hem (1970), can be indicative of saline water intrusion into the aquifer, possibly from the Caspian Sea or fossil saline water.

- Scatter plots of Na$^+$ versus Cl$^−$ reveal a linear increase in Na$^+$ with Cl$^−$, following the 1:1 line in all four aquifers. Based on the graphs drawn, in unconfined, perched, and saline aquifers, Na$^+$ and Cl$^−$ show a correlation with R^2 equal to or above 0.80 and in confined aquifers with R^2 above 0.90 (except for 2017). Therefore, it can be found that the controller process of the Cl$^−$ ion in the confined aquifer is more influenced by the Na$^+$ from fossil saline water located at the aquifer bedrock (Khairy and Janardhana 2013), whereas the Na$^+$ ion in other aquifers originates from various sources, in addition to sea salt water.

- Scatter plots of Na/Cl to Cl$^−$ can provide additional insights into the sources of Na$^+$ increase in groundwater (El-Fadel et al. 2014; Klassen et al. 2014; Sarkar et al. 2021). If this ratio is equal to one, it indicates the dissolution of halite minerals. The dissolving of other minerals and the cation exchange process can change this ratio. Since chloride is a relatively stable ion, Na/Cl > 1 can occur for two reasons: the dissolution of evaporite minerals containing Na$^+$ − SO$_4^{2-}$ and direct cation exchange between Ca^{2+} and Na$^+$ due to infiltration of freshwater (Elgettafi et al. 2012). According to the graphs drawn in the studied area, this ratio is greater than one in some wells and less than one in others. As evaporite minerals containing sodium are absent in the studied area, the
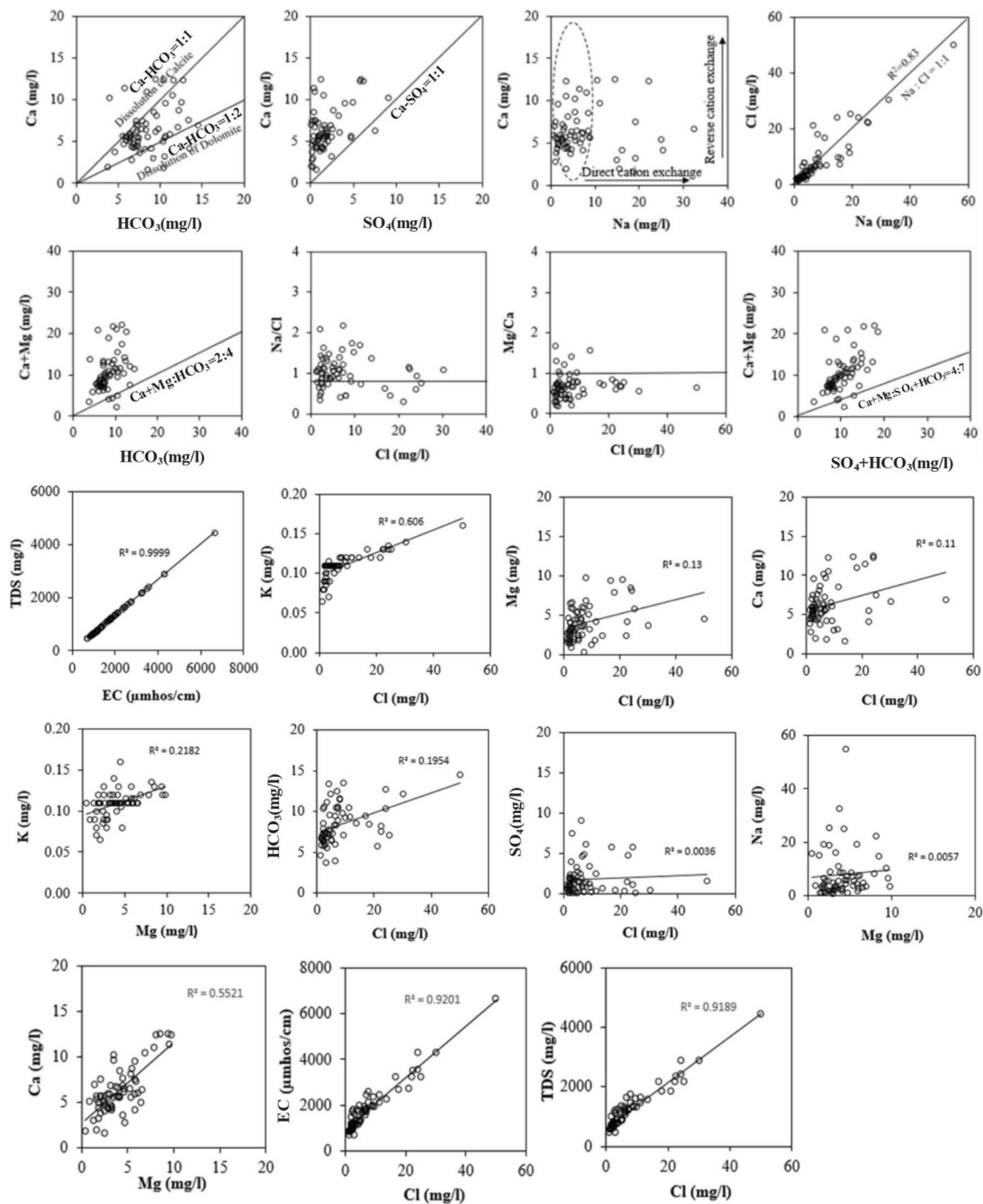
Fig. 8 Scatters plots of chemical constituent relationships in the unconfined aquifer (2011)
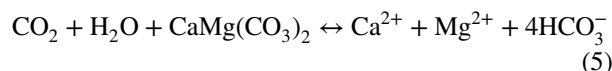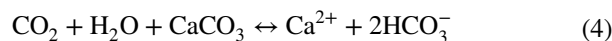
increase in the Na/Cl ratio in some wells can be attributed to direct cation exchanges due to feeding the aquifer with freshwater. Also, in wells where Na/Cl < 1, it can indicate the reverse cation exchange process due to saltwater infiltration into the coastal aquifer. Investigations on the number of samples with a Na/Cl > 1 show that their number has increased from 48 and 40% in

2011 to 60 and 53% in 2020 in unconfined and confined aquifers, respectively. This indicates the development of anthropogenic activities in creating aquifer pollution and increasing the Na/Cl ratio. When salty seawater intrudes freshwater coastal aquifers, chemical exchange processes occur between coastal aquifer rocks and seawater, resulting in calcium replacing sodium. Thus, due to the stabil-

ity of chloride concentration and sodium concentration decreases, the Na/Cl ratio decreases (Asare et al. 2021; Ghezelsofloo et al. 2021).

- Under saltwater intrusion conditions in coastal aquifers, cationic exchange reactions occur in the form of Ca–Na and Ca–Mg. During exchange reactions between cations, the concentration of sodium and magnesium decreases, and the concentration of calcium increases (Carol and Kruse 2012). Examining the Ca^{2+} versus Na scatter diagram of the studied aquifers during the years 2011, 2014, 2017, and 2020 shows the mixing process between the freshwater of the aquifer and the saltwater of the Caspian Sea. Based on these graphs, the groundwater in four aquifers shows more enrichment in Ca^{2+} than Na^+, which reflects the intrusion of saltwater (Shin et al. 2020) and reverse cation exchange in the aquifers. It should be noted that this process has also been mentioned as one of the factors of increasing salinity concentration in the aquifer in Sarkar et al. (2021) research. Nevertheless, the low correlation between chloride and calcium, suggests that, aside from seawater intrusion, other factors also contribute to the degradation of the quality of this coastal aquifer.

- The scatter diagrams of Mg/Ca versus Cl^- for both unconfined and confined aquifers during the studied period show that the average of this ratio in the unconfined aquifer for the years 2011, 2014, 2017, and 2020 is 0.66, 0.31, 0.49, and 0.48, while in the confined aquifer, it is 0.39, 0.23, 0.4, and 0.82, respectively. The ratio of Mg/Ca > 1 in the samples indicates the dissolution of dolomite in the groundwater (Elgettafi et al. 2012; Jahanshahi and Zare 2016). Given that the average of this ratio in both aquifers is less than one, it indicates that the origin of Mg^{2+} in the aquifers is not from the dissolution of dolomite but primarily reflects reverse cation exchange processes in the aquifer (Pulido-Leboeuf et al. 2003). It is worth noting that seawater typically has a high Mg/Ca ratio, ranging between 4.5 and 2.5. The low Mg/Ca ratio in the aquifer is also a result of sulfate reduction (El-Fadel et al. 2014). As the Ca/Mg ratio of the collected samples from all studied aquifers is greater than one, one of the reasons for the increase in calcium can be as a result of the seawater intrusion (Ghezelsofloo et al. 2021).

- Based on the scatter diagrams of Ca^{2+} and $Mg^{2+} + Ca^{2+}$ versus HCO_3^-, if the presence of these ions in the groundwater is the result of calcite dissolution, the plotted points should lie on a line with a slope of 1:1 (Elgettafi et al. 2012; Jahanshahi and Zare 2016). Considering that the samples of the studied area did not follow this trend and showed a weak correlation with each other, it can be concluded that the concentration of Ca^{2+} or Mg^{2+} in the groundwater has originated from other sources, such as

reverse cation exchange. Therefore, the equilibrium reaction of the calcite and dolomite dissolution/deposition process is carried out in the left direction, and as a result, the amount of HCO_3^- in the aquifer decreases (Jahanshahi and Zare 2016).

$$CO_2 + H_2O + CaCO_3 \leftrightarrow Ca^{2+} + 2HCO_3^- \tag{4}$$

$$CO_2 + H_2O + CaMg(CO_3)_2 \leftrightarrow Ca^{2+} + Mg^{2+} + 4HCO_3^- \tag{5}$$

- Soluble sedimentary minerals that can release Ca^{2+} and SO_4^{2-} ions in water due to dissolution include gypsum ($CaSO_4^{2-}.2H_2O$) and anhydrite ($CaSO_4^{2-}$). By drawing a scatter diagram of Ca^{2+} and SO_4^{2-} ions, one can determine the origin of these ions. If gypsum dissolution has occurred in groundwater, samples should be placed along the 1:1 line (Elgettafi et al. 2012). According to Fig. 8 and Figs. 1, 2, 3, 4, 5, 6 and 7 presented in part II of Supplementary information, none of the samples was located along the 1:1 line. However, all the samples were located along the vertical axis of the Ca^{2+} ion. Therefore, the Ca^{2+} concentration of the samples has increased, or the SO_4^{2-} concentration has decreased. Therefore, the origin of Ca^{2+} and SO_4^{2-} ions cannot be attributed to the dissolution of gypsum and anhydrite minerals. The low concentration of SO_4^{2-} may be a result of biological reduction in the region. Also, the increase in Ca^{2+} can be related to the dissolution of calcite dolomite, as well as reverse cation exchange reactions. Based on the results of scatter diagrams for Ca^{2+} and $Ca^{2+} + Mg^{2+}$ versus HCO_3^- in the studied area, the only plausible reason for the rise in Ca^{2+} appears to be reversed cation exchanges reactions. In order to investigate the cause of the increase in the Ca^{2+} and Mg^{2+} ions as a result of the dissolution of calcite and dolomite or other minerals, the scatter diagram of $Ca^{2+} + Mg^{2+}$ vs $SO_4^{2-} - HCO_3^-$ was drawn. If the dissolution of calcite, dolomite, and gypsum are in equilibrium conditions, the samples are drawn along a line with a slope of 4:7, and the following relationship is established (Jahanshahi and Zare 2016):

$$3CO_2 + 3H_2O + CaCO_3 + CaMg(CO_3)_2 + CaSO_4 \leftrightarrow 3Ca^{2+} + Mg^{2+} + 6HCO_3^- + SO_4^{2-} \tag{6}$$
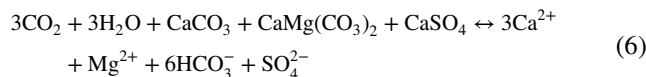
The scatter diagrams that are drawn in Figs. 6, 7, 8, 9, 10, 11, 12 and 13 show that most of the samples are on the left side of this line, and based on this, it can be concluded that in the studied area, the source of increasing the concentration of Ca^{2+}, Mg^{2+}, and SO_4^{2-} ions are not the dissolution of calcite, dolomite, and gypsum minerals.
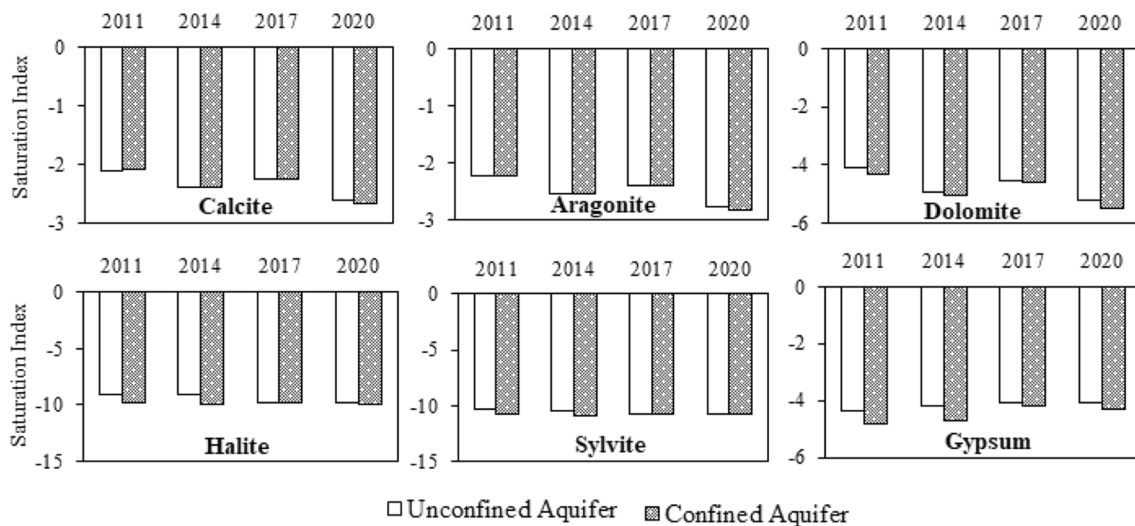
Fig. 9 Mean saturation indices of evaporate minerals in the unconfined and confined aquifers of GH.-J. plain (from 2011 to 2020)

In order to confirm the results of the scatter plots and ion ratios, the saturation index (*SI*) is calculated. Saturation index can show the effect of rock weathering on water chemistry and can be measured with the help of Eq. 7 (Ghosh et al. 2022; Zhang et al. 2020).

$$SI = \frac{K_{IAP}}{K_{SP}} \tag{7}$$

where K_{IAP} and K_{SP} are ion's activity products for a mineral reaction and the solubility product of that mineral, respectively. The PHREEQC software (v. 3.3.7) is handy for calculating the *SI* of minerals in the water (Parkhurst and Appelo 1999). The *SI* value indicates the nature of water and mineral chemical equilibrium with water–rock interaction. $SI < 0$ indicates an unsaturated state where the minerals undergo continuous weathering by the groundwater or surface water; Conversely, $SI > 0$ states the supersaturated state when the minerals start to precipitate. Moreover, *SI* close to 0 indicates the equilibrium states of the mineral phase.

The values of the saturation index of every mineral genuinely represent the actual phenomena of rock-water interaction and their contribution to the evolution of groundwater hydrochemistry. The *SI* values for calcite, aragonite, dolomite, halite, sylvite, and gypsum in both unconfined and confined aquifers consistently fall within the negative range, signifying an unsaturated state. Therefore, the dissolution of these minerals can determine the amount of Na^+, K^+, Ca^{2+}, Mg^{2+}, SO_4^{2-}, Cl^-, and HCO_3^- in the groundwater in both aquifers. Nevertheless, considering that there are no evaporate formations such as halite, sylvite, gypsum, and anhydrite in the case study, it can be concluded that significant concentrations of Na^+, K^+, Ca^{2+}, Mg^{2+}, Cl^-, and SO_4^{2-}

are attributable to saline fluids from fossil aquifer and the intrusion of saltwater.

Due to the higher *SI* for calcite and aragonite minerals compared to other minerals in the recharge zone (located in the southern part of the plain), the effect of the dissolution of carbonate-containing rocks (the limestone and marl formations of the highlands) on the development of groundwater is determined. The higher value of the *SI* of the confined aquifer, compared to the unconfined aquifer, shows that this aquifer is more affected by the intrusion of saltwater and fossil saline aquifer (Fig. 9).

Major controllers on groundwater chemical composition in the GH.-J. plain aquifers

Pearson's correlation matrix analysis (CMA) was performed to find relationships between two or more variables using IBM Statistic SPSS 26.0 software in unconfined and confined aquifers during the years 2011, 2014, 2017, and 2020 (Tables 1, 2, 3, 4, 5, 6 and 7, along with Table 4 (refer to supplementary information Part II for details)). It should be noted that the correlation value greater and smaller than 0.6 indicates a strong and weak correlation between the variables, respectively (Elgettafi et al. 2012). Considering the strong correlation of EC with HCO_3^-, Na^+, K^+, Cl^-, and TDS, it can be found that these parameters are the main sources of salinity in the studied area. Also, these parameters show a strong correlation with each other. This shows that the water of different samples has similar geochemical properties. Also, the strong correlation of these parameters with Cl^- suggests minimal interaction of water with the rocks in the porous media since the water enters the aquifers.
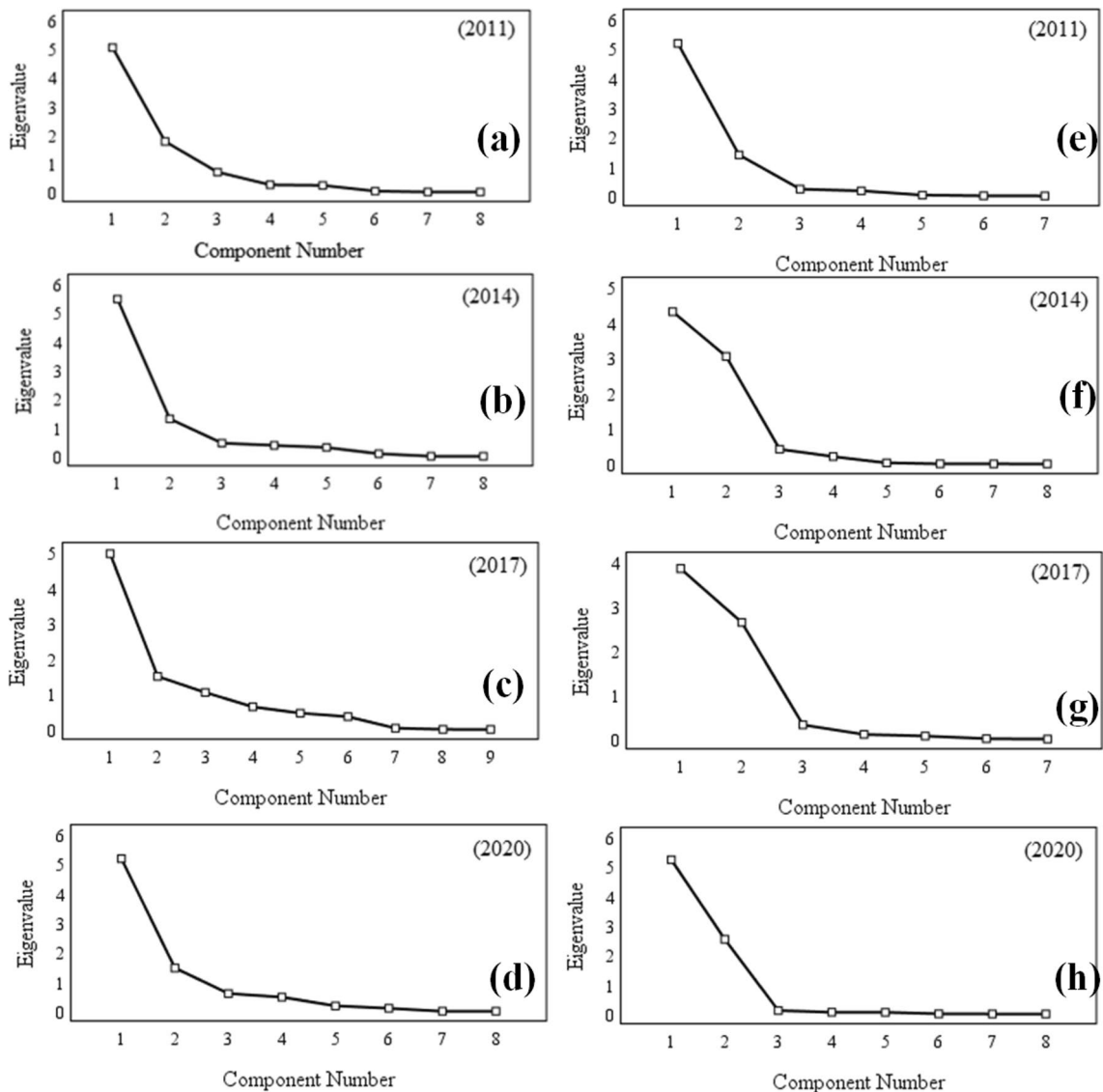
Fig. 10 Scree plots of the physicochemical variables in the unconfined aquifer (**a**, **b**, **c**, and **d**) and confined aquifer (**e**, **f**, **g**, and **h**)

In order to investigate the main factors controlling the chemical composition of groundwater in the unconfined and confined aquifers and their variations during the study period, principal component analysis (PCA) was applied to all samples. The results of the Scree test, as shown in Fig. 10, confirm that only the two first principal components should be considered as salinity factors. This implies that the controlling factors for salinity, with the exception of the unconfined aquifer in 2017) are reduced to two components. Because the eigenvalue accounted by the third component is smaller than the minimum eigenvalue (i.e., 1), it is ignored. This factor analysis reduced the dimensions of 13 physicochemical parameters to two principal components (PCs) that account for more than 83% of the variance of the entire data set during different years. In this analysis, a factor loading

greater than $+0.6$ is considered significant (Elemile et al. 2021). Consequently, only parameters deemed significant based on the factor load value are presented in Table 8 and 9 (refer to supplementary information part II). The Varimax loading of the physicochemical variable's factors in three-dimensional space is shown in Fig. 11. It should be noted that analysis of main components in saline and perched aquifers has not been applicable due to the minimal number of samples.

In an unconfined aquifer in 2011, the first principal component (PC1) shows a significant and high positive factor loading with Na^+, K^+, Cl^-, TDS, and EC and includes 55.86% of the variance of the entire dataset. The high positive correlation between the parameters Na^+, K^+, Cl^-, TDS, and EC and the lack of significant correlation
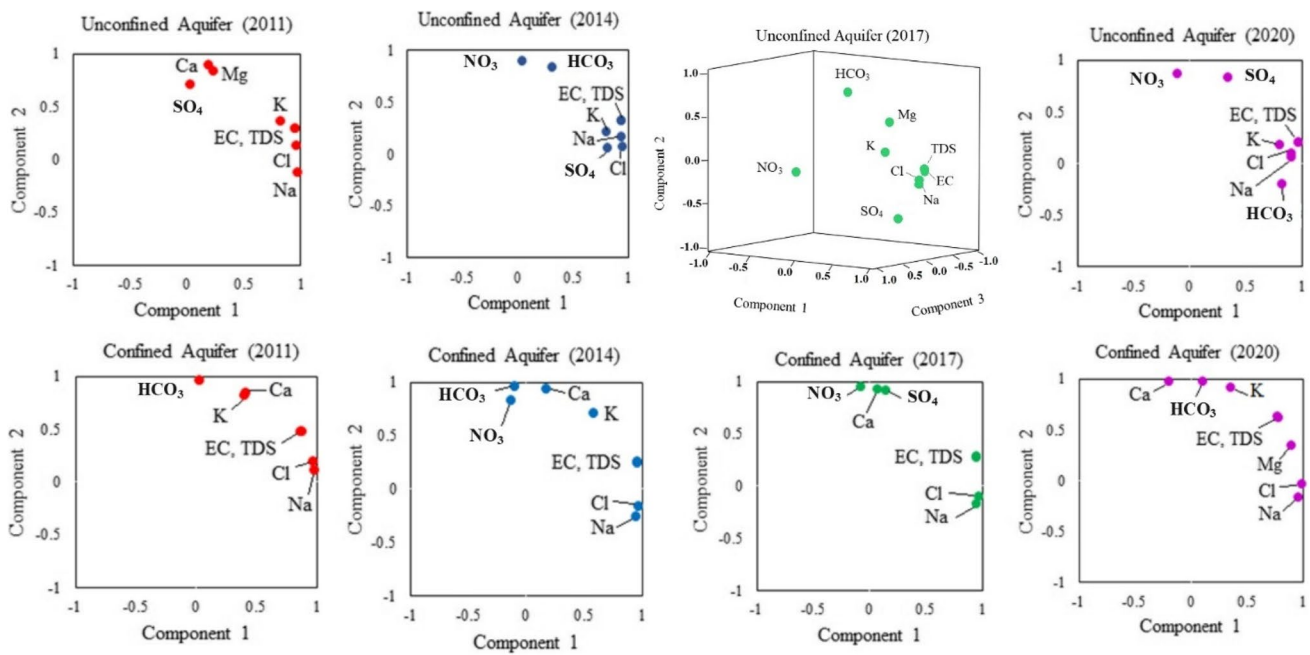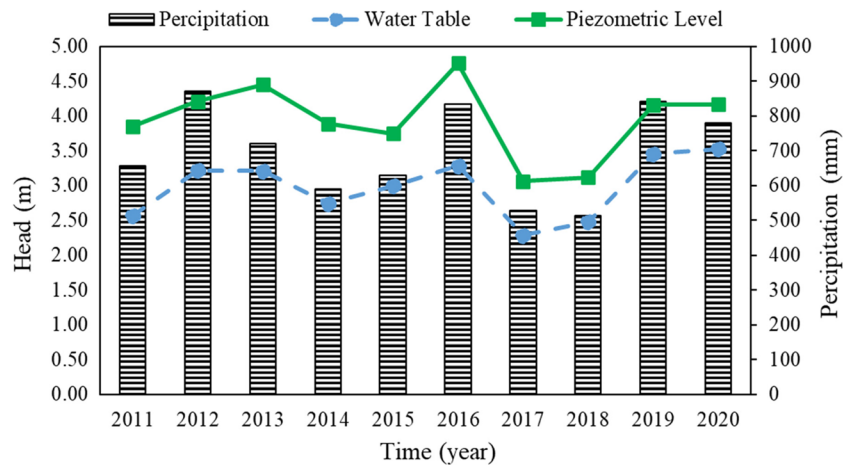
Fig. 11 Varimax loading of the physicochemical variable's factors in three-dimensional space in the confined and unconfined aquifer

Fig. 12 Variations of precipitation, measured water table, and piezometric level in the confined and unconfined aquifers of GH.-J. aquifer (2011–2020)


between Cl^- and Ca^{2+}, Mg^{2+}, and SO_4^{2-} indicate that the first source of the salinity of this aquifer in 2011 is the infiltration of fossil saline water from bedrock and seawater intrusion. The second factor, which accounts for about 29.14%, includes Ca^{2+}, Mg^{2+}, and SO_4^{2-} parameters. Chloride has not shown a strong significant correlation with these parameters, and therefore, it cannot originate from seawater or fossil saline water. On the other hand, based on the scatter diagrams drawn in the previous section, the factor of producing these parameters cannot be the dissolution of minerals such as calcite, dolomite, and gypsum. Based on the available evidence, it can be concluded that the second source of groundwater salinity in 2011 was

the reverse cation exchange process due to the favorable lithological conditions in the aquifer (the presence of clay minerals and carbonaceous organic materials).

In 2014, PC1 shows a significant positive factor loading with Na^+, Cl^-, EC, TDS, K^+, SO_4^{2-}, and includes 62.14% of the total data variance. The high positive correlation between the parameters Na^+, Cl^-, EC, TDS, K^+, and SO_4^{2-} and the lack of significant correlation between Cl^-, NO_3^-, and HCO_3^- indicate that the first source of groundwater salinity in the unconfined aquifer in 2014 is seawater and fossil saltwater trapped in the coastal unconfined aquifer sediments. In fact, since 2013, due to the establishment of the water supply network of the Alborz dam (WSNA) in the plain, the use

Fig. 13 Representation of groundwater sampled from four aquifers in **a** 2011, **b** 2014, **c** 2017, and **d** 2020 on Piper diagram
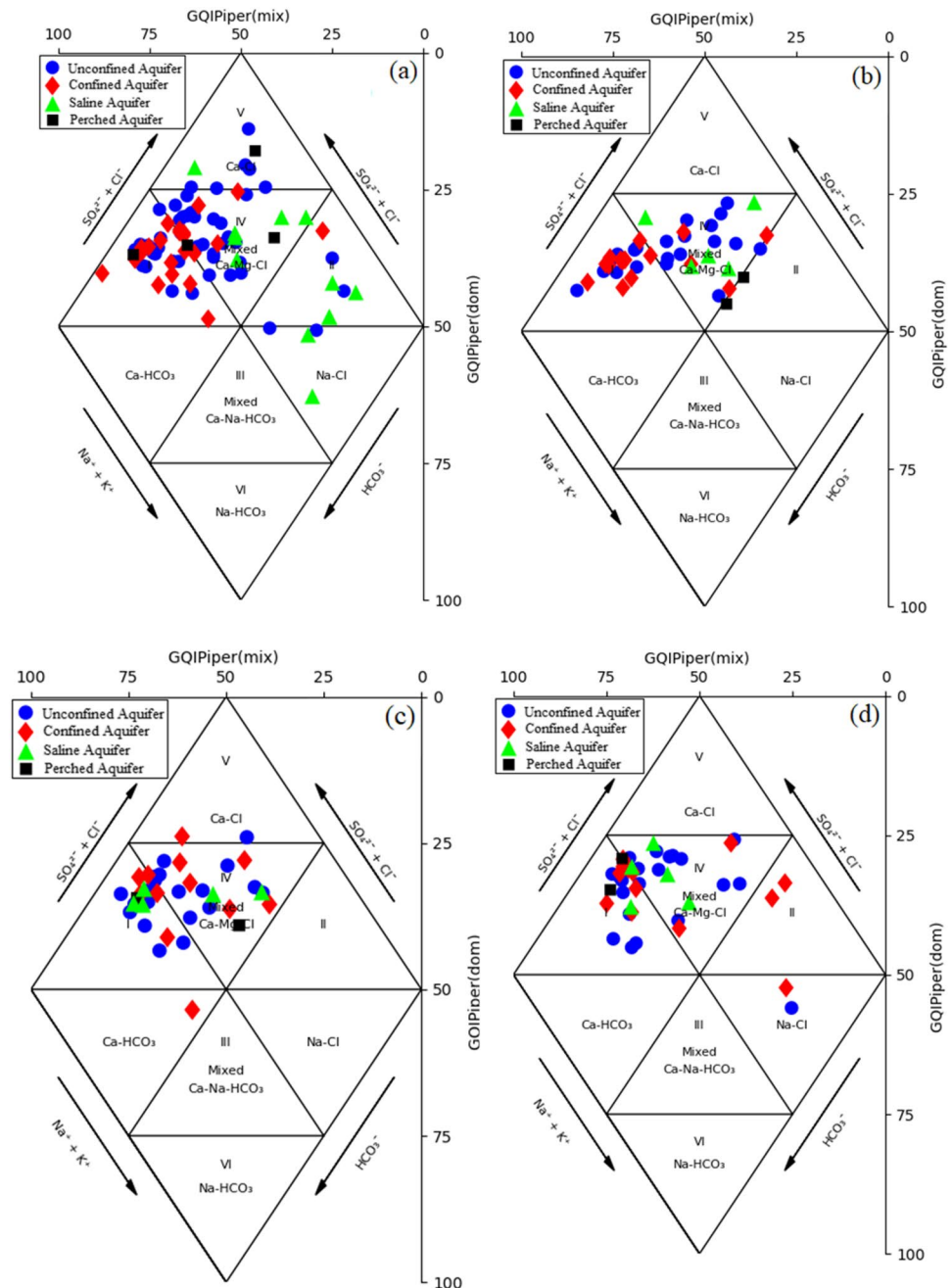
of groundwater for agriculture has been reduced (shahnazari et al. 2018). As a result, it has prevented the entry of seawater and fossil saltwater from bedrock into the aquifer. Therefore, salty waters that have already remained among the sediments are considered the first salinity cause this year. The second factor, which accounts for 22.5%, includes NO_3^- and HCO_3^- parameters. Similar to the reasons presented in the second factor related to 2011, the origin of these parameters is not from seawater or fossil saline water. Also, based on the scatter diagrams of Ca^{2+} and $Mg^{2+} + Ca^{2+}$ versus HCO_3^- and the existence of a weak correlation between them, the cause of HCO_3^- production cannot be the dissolution of

minerals such as calcite, dolomite, and gypsum. Based on the available evidence, it can be concluded that the second source of salinity in 2014 is the high volume of sugar urea fertilizer consumption (with 46% absorbable nitrogen content) in rice fields and the penetration of nitrates into the groundwater through agricultural return flow (affected by the establishment of the WSNA since 2013).

In 2017, the PC1 showed a significant and high positive factor loading with Na^+, Cl^-, EC, TDS, K^+, and SO_4^{2-} and accounts for 52.610% of the total data variance. The strong positive correlation among these parameters, along with the absence of a significant correlation between Cl^-

Table 4 Pearson's correlation matrix of the unconfined aquifer hydrochemical parameters in 2011

Parameters	SO_4^{2-}	Cl^-	HCO_3^-	pH	TDS	Th	SAR	EC	K^+	Na^+	Mg^+	Ca^{2+}
SO_4^{2-}	1											
Cl^-	0.06	1										
HCO_3^-	0.07	0.44**	1									
pH	−0.18	0.17	−0.10	1								
TDS	0.25*	0.96**	0.62**	0.09	1							
Th	0.46**	0.37**	0.39**	−0.18	0.49**	1						
SAR	−0.04	0.78**	0.44**	0.25*	0.75**	−0.17	1					
EC	0.25*	0.96**	0.62**	0.08	1.00**	0.49**	0.75**	1				
K^+	0.27*	0.78**	0.64**	0.08	0.86**	0.49**	0.62**	0.86**	1			
Na^+	0.06	0.91**	0.52**	0.18	0.90**	0.06	0.94**	0.90**	0.73**	1		
Mg^+	0.38**	0.36**	0.39**	−0.17	0.47**	0.92**	−0.13	0.46**	0.47**	0.08	1	
Ca^{2+}	0.48**	0.33**	0.33**	−0.16	0.45**	0.95**	−0.19	0.44**	0.45**	0.04	0.74**	1

*Correlation is significant at alpha ≤ 0.05 level; **correlation is significant at alpha ≤ 0.01 level

Table 5 Main pollution sources governing the quality of GH.-J. plain aquifers

	Source of pollution in two aquifers			
year	Unconfined		Confined	
	Primary	Secondary	Primary	Secondary
2011	Hydro-geochemical and Geogenic processes (seawater intrusion and fossil waters trapped between sediments)	Geogenic and hydro-geochemical processes	Geogenic process (local upconing of underlying fossil saline water due to extra discharge from agriculture wells)	Geogenic and hydro-geochemical process
2014		Anthropogenic processes (Agricultural activities and domestic wastewater)		Anthropogenic process (Agricultural activities)
2017		Geogenic, hydro-geochemical, and Anthropogenic processes	Geogenic process (upconing progress of underlying fossil saline water to confined aquifer)	Anthropogenic process (Agricultural activities and domestic wastewater)
2020		Anthropogenic process (Agricultural activities and domestic wastewater)		Geogenic and hydro-geochemical processes

Table 6 Water type in all wells in unconfined, confined, saline, and perched aquifers based on the Piper diagram using $GQI_{\text{Piper(mix)}}$ and $GQI_{\text{Piper(dom)}}$ indices in 2011, 2014, 2017, and 2020

Year	Aquifer type							
	Unconfined		Confined		Saline		Perched	
	Type	Percent	Type	Percent	Type	Percent	Type	Percent
2011	Ca–HCO$_3$	34.78	Ca–HCO$_3$	81.82	Na–Cl	50	Ca–HCO$_3$	50
	Mixed Ca–Mg–Cl	50	Mixed Ca–Mg–Cl	13.64	Mixed Ca–Mg–Cl	41.60	Mixed Ca–Mg–Cl	25
	Na–Cl	8.70	Na–Cl	4.54	CaCl	8.40	CaCl	25
	CaCl	6.52						
2014	Ca–HCO$_3$	38.10	Ca–HCO$_3$	73.40	Mixed Ca–Mg–Cl	100	Mixed Ca–Mg–Cl	100
	Mixed Ca–Mg–Cl	57.10	Mixed Ca–Mg–Cl	13.30				
	Na–Cl	4.80	Na–Cl	13.30				
2017	Ca–HCO$_3$	52.38	Ca–HCO$_3$	50	Ca–HCO$_3$	60	Ca–HCO$_3$	50
	Mixed Ca–Mg–Cl	47.62	Mixed Ca–Mg–Cl	50	Mixed Ca–Mg–Cl	40	Mixed Ca–Mg–Cl	50
2020	Ca–HCO$_3$	42.85	Ca–HCO$_3$	61.50	Ca–HCO$_3$	40	Ca–HCO$_3$	100
	Mixed Ca–Mg–Cl	52.40	Mixed Ca–Mg–Cl	15.40	Mixed Ca–Mg–Cl	60		
	Na–Cl	4.80	Na–Cl	23.10				

and other parameters, indicates that the utilization of water from the WSNA on the plain, coupled with reduced groundwater extraction, has stopped the penetration of salty water from the sea and bedrock to the coastal aquifer. As a result, the first source of salinity in the unconfined aquifer in 2017 is similar to the salinity source in 2014. In 2017, PC2 accounted for 18.7% of the total variance and included HCO_3^- and Mg^{2+} parameters. The absence of a strong significant correlation of chloride with these parameters, and also based on a scatter plot ($Ca^{2+} + Mg^{2+}$) to HCO_3^-, can be seen that the origin of these parameters is not from seawater, fossil saline water, and dissolution of dolomite. Therefore, the second salinity factor in 2017 was reverse cation exchange in the unconfined aquifer. The third principal component (PC3) shows a significant and high positive factor loading with NO_3^- and includes 12.08% of the variance of the entire data set. As this parameter has not demonstrated a strong and significant correlation with other parameters, the presence of nitrate can be attributed to agricultural activities and the extensive use of nitrate fertilizers, leading to their infiltration into groundwater through agricultural return flow. On the other hand, the establishment of the WSNA in 2013 has been effective in better transfer of nitrate in chemical fertilizers to groundwater.

In 2020, the PC1 showed a significant and high positive factor loading with Na^+, Cl^-, EC, TDS, K^+, and HCO_3^- and accounting for 62.97% of the total data variance. The high positive correlation between these parameters together and the lack of significant correlation between Cl^-, NO_3^-, and SO_4^{2-} indicate that the primary source of the salinity of the unconfined aquifer in 2020 is still sea saltwater and fossil waters trapped in the sediments of this aquifer. The PC2 with accounting for 20.06% includes NO_3^- and SO_4^{2-} parameters. Chloride does not show a strong significant correlation with these parameters, so the origin of these parameters cannot be from seawater or fossil saline water. On the other hand, the weak correlation between Ca^{2+} and SO_4^{2-} shows that the origin of the SO_4^{2-} cannot be from the dissolution of gypsum. Therefore, the sole factor capable of elevating the concentration of NO_3^- and SO_4^{2-} is the extensive use of nitrated chemical fertilizers, triple superphosphate (a combination of sulfuric acid and natural phosphate), and potassium sulfate in agricultural lands.

Through statistical and factor analysis conducted on the unconfined aquifer samples over a 10-year period, it is evident that the main factors of salinity and the variations in water chemical composition of this aquifer differ across various years. The entry of saline water from the Caspian Sea into the unconfined aquifer and the rise of fossil saline water from the bedrock under the influence of the increase in the exploitation of agricultural wells were identified as the leading causes of salinity in all the studied years. The variation of groundwater level and piezometric level (Fig. 12) shows

that the piezometric surface of the confined aquifer is higher than the water level of the unconfined aquifer. Therefore, according to the geological and lithological conditions in the studied area, there is a possibility of saltwater leakage from the salted confined aquifer to the unconfined aquifer in the parts where there are leakage layers.

In 2011 and 2017, the reverse cation exchange process, and in 2014 and 2020, the impact of domestic sewage, agricultural activities, and nitrate-containing chemical fertilizers were identified as the second factor of salinity and changes in the chemical composition of an unconfined aquifer. In 2017, agricultural activities and the extensive use of nitrate fertilizers were considered as the third factor of salinity. Therefore, the parameters of the first factor during these 10 years, as well as the parameters of the second factor in the years 2011 and 2017, according to their origin, indicate the general trend of groundwater (natural) and the influence of geological formations on it (Geogenic and hydro-geochemical processes). The effective parameters in the second factor in 2014 and 2020 and the third-factor parameter in 2017 show the effect of human or agricultural activities (anthropogenic origin) in increasing salinity (Table 5).

In this section, the results of the PCA on the confined aquifer samples in 2011, 2014, 2017, and 2020 are described as follows.

In the confined aquifer in 2011, the first rotated component (PC1) shows a positive, significant, and high factor loading with Na^+, Cl^-, EC, and TDS and accounting for 54.1% of the total data variance. The high positive correlation between these parameters together and the lack of significant correlation between Cl^-, Ca^{2+}, K^+, and HCO_3^- indicates that although the water quality of this aquifer has been good until 2011, evidence of the progress of the intrusion phase can be seen in it. Therefore, the first source of the groundwater salinity of this aquifer in 2011 is the upcoming of the deep saline water into the confined aquifer under the influence of excessive groundwater pumping by agricultural wells in some parts of the plain. The second rotated component (PC2) which accounts for 39.69%, has strong positive loading with Ca^{2+}, K^+, and HCO_3^-. Therefore, it can be concluded that the second source of groundwater salinity in 2011 was reverse cation exchange due to the local upcoming of fossil saline water from bedrock to the confined aquifer and under favorable lithological conditions.

In 2014 and 2017, PC1 showed a positive, significant, and high factor loading with Na^+, Cl^-, EC, and TDS, accounting for 51.75% and 52.86% of the total data variance, respectively. There is a high positive correlation between parameters Na^+, Cl^-, EC, and TDS, together, expressing the local progress of the intrusion phase and the rise of fossil saline water from the bedrock in 2014 and its development in 2017. Also, in 2014 and 2017, PC2 accounted for
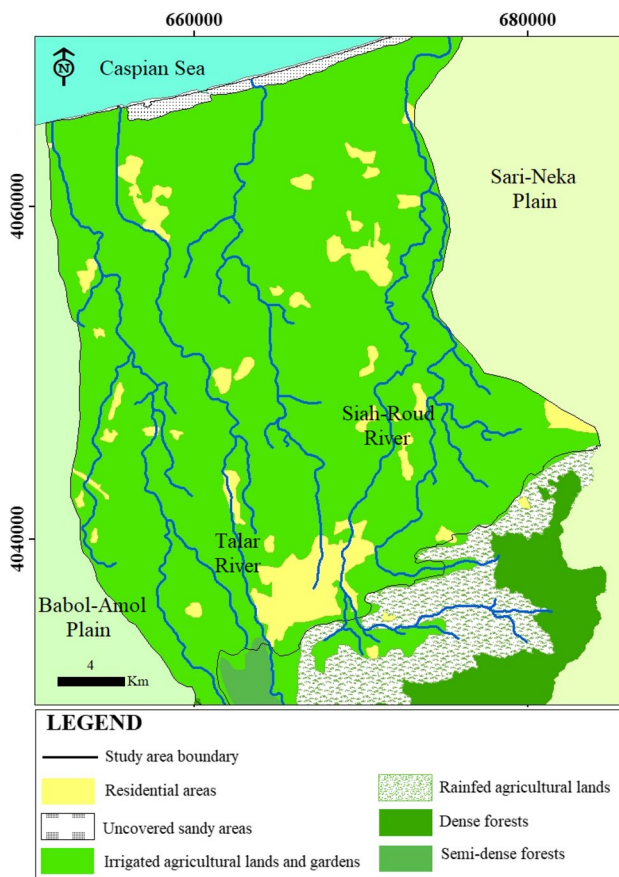
Fig. 14 Representation of land-use map of the case study

40.07% and 39.9% of the total data variance, respectively. Considering the influential parameters within this factor, the second source of aquifer salinity encompasses domestic sewage, agricultural activities, and the extensive use of nitrate-containing chemical fertilizers, triple superphosphate (a combination of sulfuric acid and natural phosphate), and potassium sulfate.

The evaluation of the PC1 of 2020 shows that there is a high positive correlation between Na^+, Cl^-, EC, TDS, and Mg^{2+} parameters. Also, there is no significant correlation between Cl^- with Ca^{2+}, K^+, and HCO_3^-. Therefore, the progression of the intrusion phase and the rise of fossil saline water continues. According to PC2, the second source of confined aquifer salinity in 2020 is the progress of reverse cation exchanges due to the intrusion of fossil saline water.

Based on the statistical and factor analysis performed on the confined aquifer samples in 10 years, two main factors were identified for the origin of salinity and the change in the chemical composition of this aquifer. The rising fossil saline water from bedrock under the influence of increasing operation of agricultural wells is considered the first factor of salinity. The second most effective factor in 2011 and 2020 is associated with the reverse cation exchange process.

In contrast, in 2014 and 2017, domestic wastewater, agricultural activities, and the use of nitrate fertilizers emerge as the primary contributors to this factor. Therefore, according to their origin, the factors of confined aquifer salinity in 2011 and 2020 were geogenic and hydro-geochemical, and in 2014 and 2017, they were anthropogenic (Table 5).

Evolution of potential seawater intrusion based on Piper diagram and GQI_{SWI} index.

By calculating the groundwater quality indicators $GQI_{Piper(mix)}$ and $GQI_{Piper(dom)}$ based on the quality samples collected from four aquifers during the years 2011, 2014, 2017 and 2020, the modified Piper diagram was drawn according to Fig. 13. Also, the spatiotemporal distribution of the obtained water types for the four studied aquifers is presented in Figs. 15 and 16.

The separated results of the water quality type based on this diagram (Table 6) show that in the unconfined aquifer in 2011, 50% of the samples were in IV (mixed Ca–Mg–Cl waters), which these conditions reflect the visible impact of the intrusion phenomenon and the reverse cation exchange process in this coastal aquifer.

In 2014, 57.10% of the samples were in IV (Ca–Mg–Cl mixed waters), and 38.10% of samples were in I (freshwater). According to the increase in the percentage of samples located in the IV and I zones compared to 2011, it can be found that the intrusion process and the invasion of the saltwater in the unconfined aquifer from 2011 to 2014 experienced a decrease. This receding in the saline water intrusion has been affected by the establishment of the WSNA in the plain since May 2013 (Table 6) and the use of surface water in the irrigation of agricultural lands and gardens (by covering more than 98% of the plain area) (Fig. 14). These conditions indicate the ability of the freshwater to push back the saltwater front.

Table 7 The performance of the WSNA in the Ghaemshahr-Juybar plain

Year	Inlet water (MCM)	Consumption amount (MCM)		
		Agriculture	Aquaculture	Other water catchments
2013	11.01	10.45	0	0
2014	**21.476**	**18.184**	**1.145**	**0**
2015	64.907	52.431	0	0
2016	20.126	14.760	0	1.280
2017	**66.150**	**52.920**	**0**	**0**
2018	59.580	47.664	0	0
2019	24.790	19.832	0	0
2020	**38.950**	**31.160**	**0**	**0**
2021	89.370	69.160	0	2.336

Bold rows indicate the studied years in Ghaemshahr-Juybar plain

Fig. 15 Spatial distribution of water chemistry types in GH.-J. plain based on Piper diagram using $GQI_{\text{Piper(mix)}}$ and $GQI_{\text{Piper(dom)}}$ indices in the perched, saline, and unconfined aquifers in **a** 2011, **b** 2014, **c** 2017, and **d** 2020
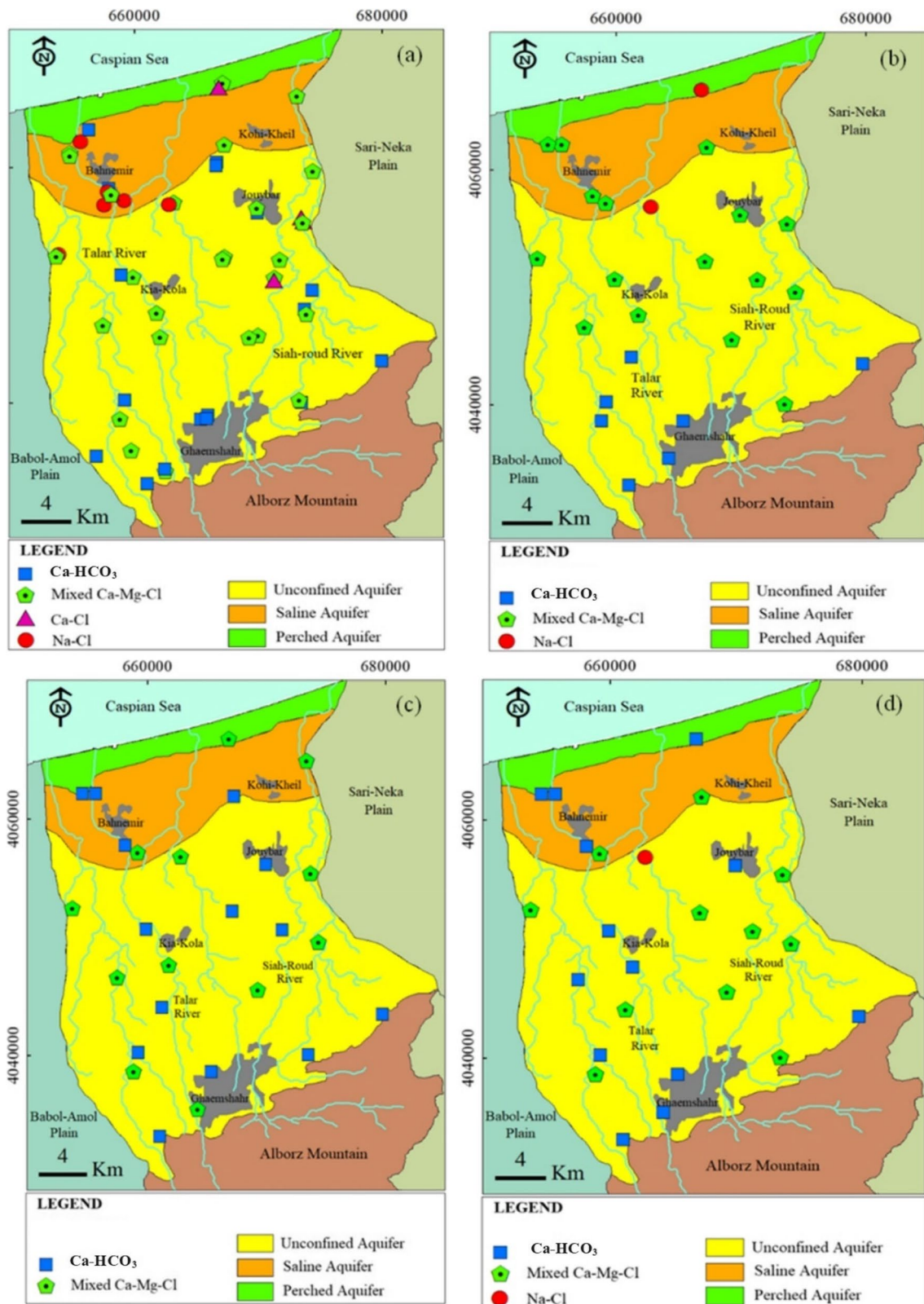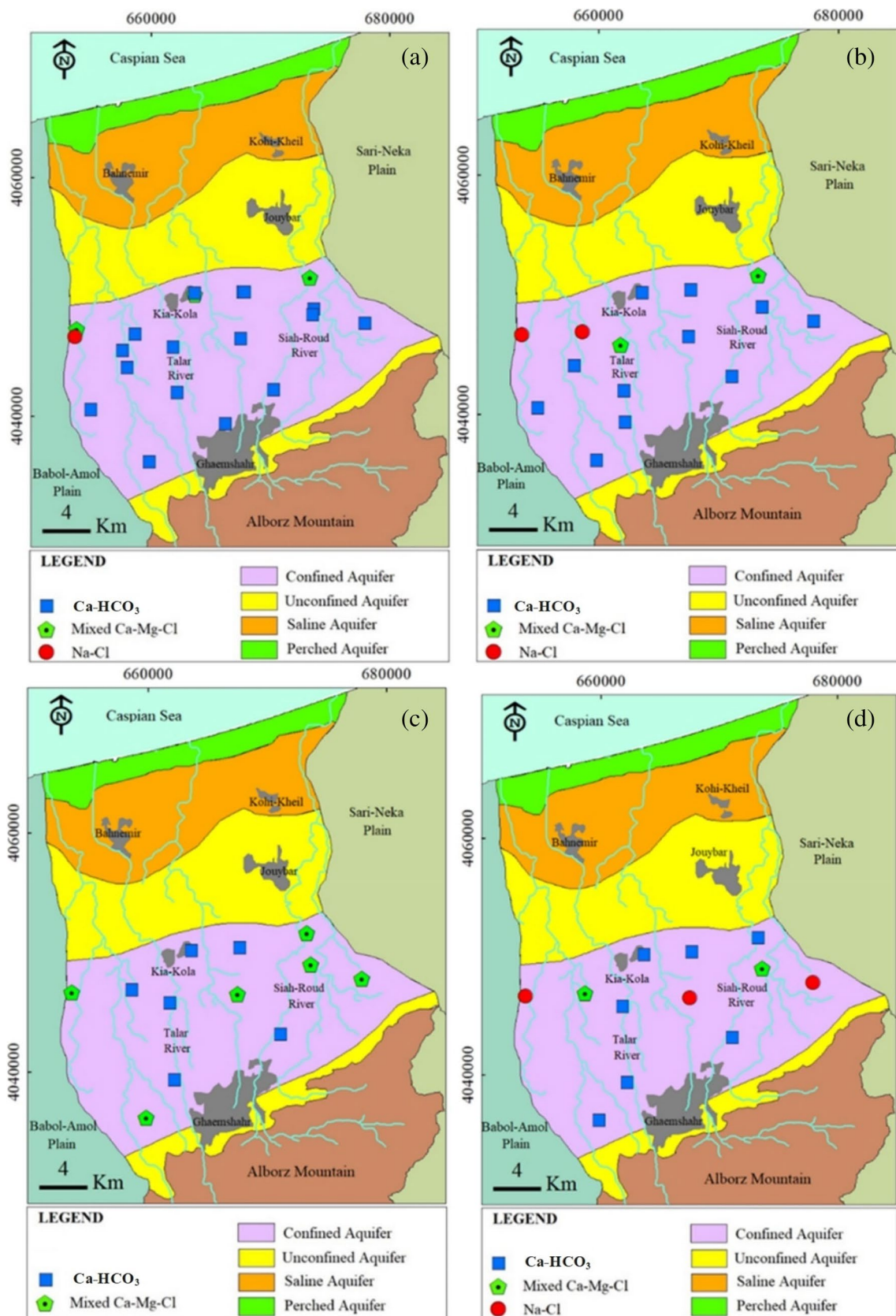
Fig. 16 Spatial distribution of water chemistry types in GH.-J, plain based on Piper diagram using $GQI_{Piper(mix)}$ and $GQI_{Piper(dom)}$ indices in the confined aquifer in **a** 2011, **b** 2014, **c** 2017, and **d** 2020

From the increase in the percentage of samples located in zone I (freshwater) in 2017 compared to 2014, it can be seen that the effects of the WSNA are continuing in the pushing back the seawater intrusion (Table 7). In 2020, 52.4% and 4.8% of the samples were in zone IV (Ca–Mg–Cl mixed waters) and zone II (water salt), respectively. Therefore, intrusion on the plain has slightly increased from 2017

to 2020 due to decreased in inflow from WSNA in 2020 (Table 7; Fig. 15).

The only fresh aquifer in the studied area is the perched aquifer, located at the shortest distance from the Caspian Sea. However, the water in this aquifer has consistently remained fresh in all years, thanks to the presence of an alluvial layer covering the clay lenses. Although the effects
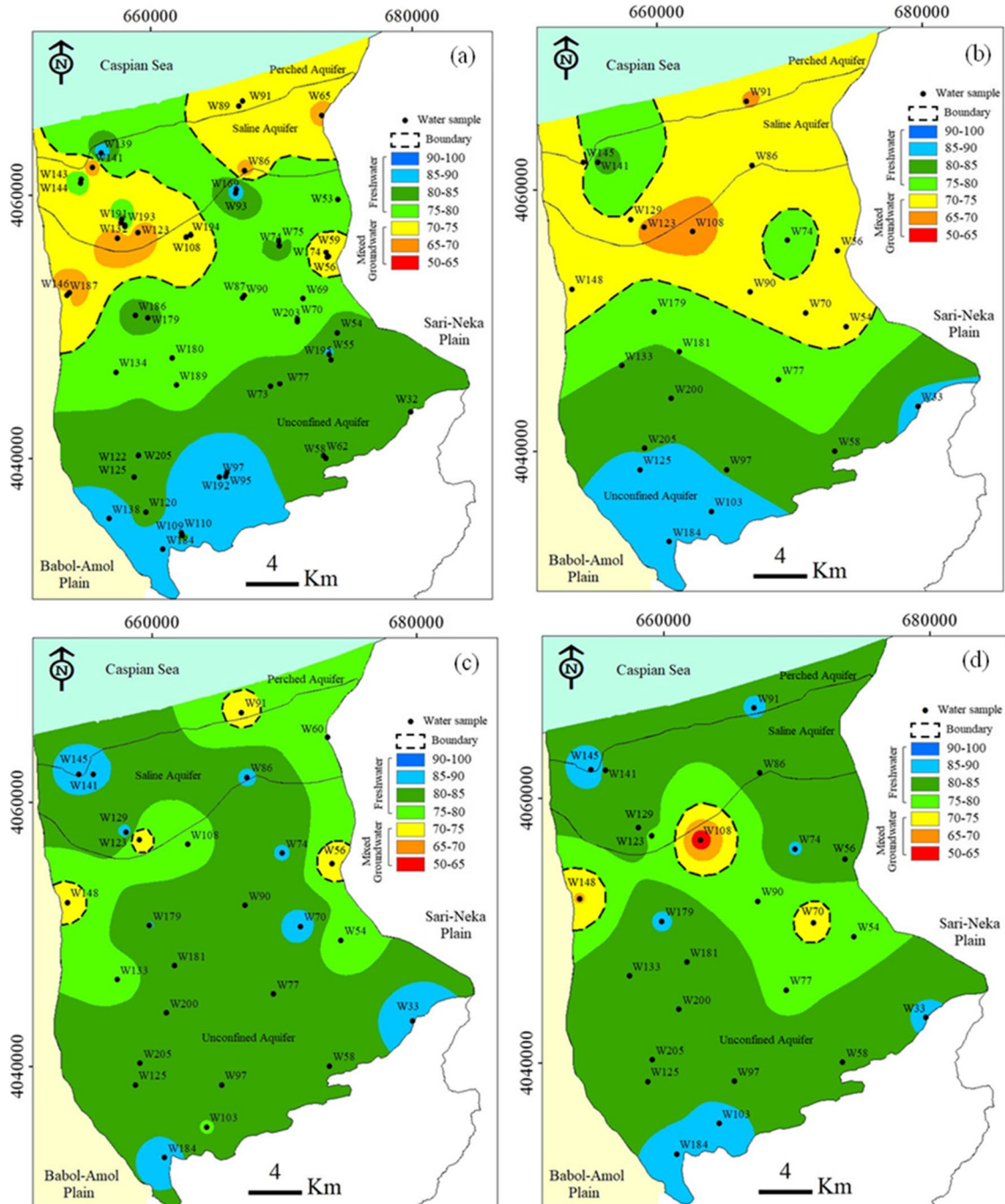

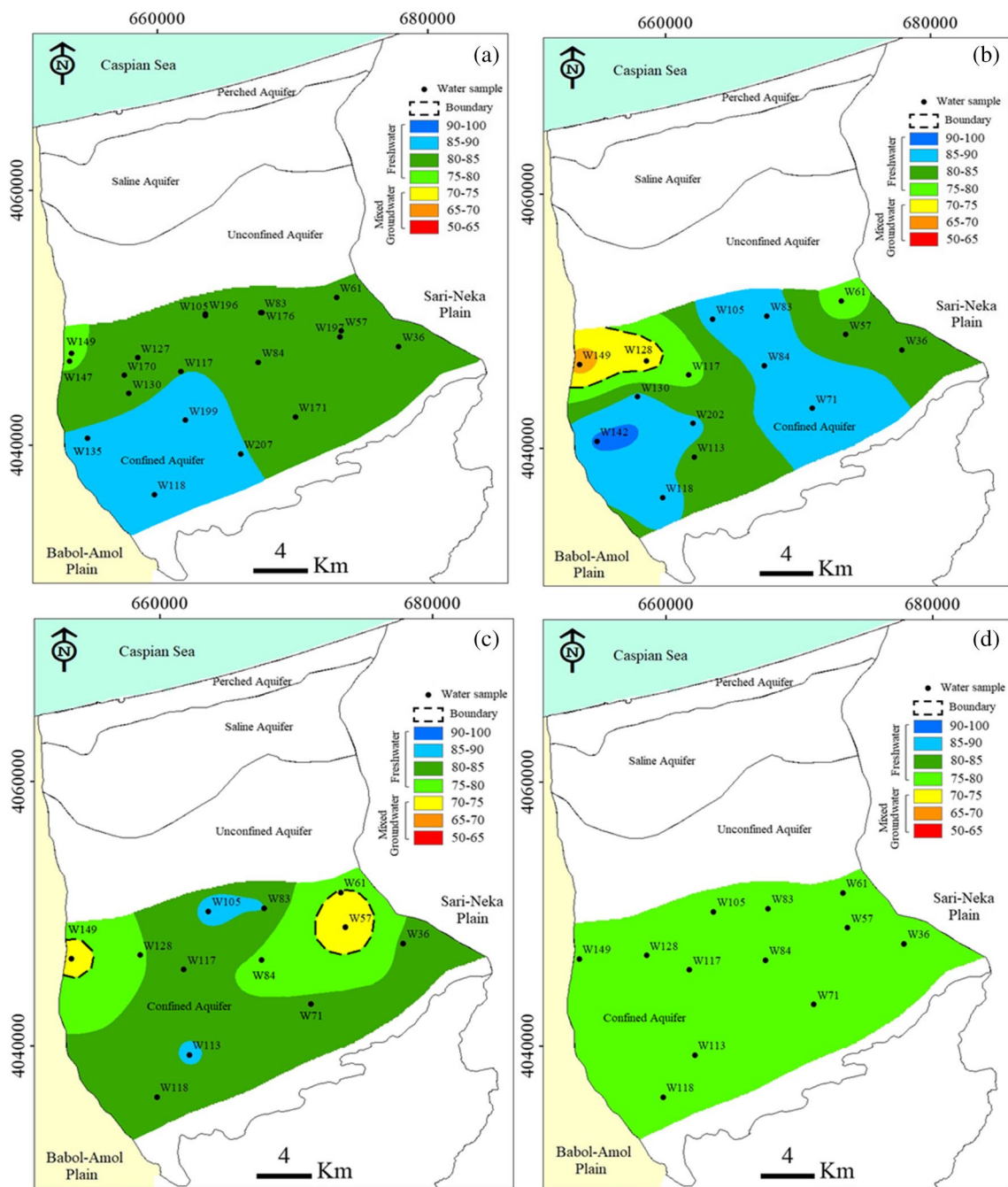**Fig. 17** Spatial distribution of GQI_{SWI} index in perched, saline, and unconfined aquifers for 2011 (**a**), 2014 (**b**), 2017 (**c**), and 2020 (**d**)

Fig. 18 Spatial distribution of GQI_{SWI} index in the confined aquifer for 2011 (**a**), 2014 (**b**), 2017 (**c**), and 2020 (**d**)

of intrusion were observed in 2011 and 2014, during the following years, the amount of intrusion decreased so that in 2020, $Ca-HCO_3$ was the dominant water type detected in this aquifer. Field investigations show that the chemical composition of this aquifer has also been improved with the establishment of the WSNA and the use of surface water in the irrigation of agricultural lands and gardens during these years.

The saline aquifer, located between the perched and unconfined aquifer, has consistently exhibited salinity over the years. However, similar to other aquifers in the plain, the salinity of this aquifer has been affected by the establishment of the WSNA. From 2014 to 2020, it has experienced a sharp decrease in salinity, leading to an improvement in groundwater quality (Fig. 15).

Table 8 Results of GQI_{SWI} index for GH.-J. groundwater samples in 2011, 2014, 2017, and 2020

Aquifer type	Water type	Typical GQI_{SWI}		GQI_{SWI} index for GH.-J. groundwater samples																
		Min	Max	2011				2014				2017				2020			
				Min	Max	Mean	(%)	Min	Max	Mean	(%)	Min	Max	Mean	(%)	Min	Max	Mean	(%)
Unconfined	FW	75	100	75.03	89.58	82.53	79.17	77.52	92.52	84.42	66.67	76.31	88.58	83.67	78.26	76.50	86.79	83.58	82.60
	MGW	50	75	60.92	74.77	72.82	20.83	67.51	74.24	72.49	33.33	64.13	74.97	71.49	21.74	62.68	71.92	70.06	17.40
	SGW	10	50	-	-	-	-	-	-	-	-	-	-	-	-	-	-	-	-
	SW	0	10	-	-	-	-	-	-	-	-	-	-	-	-	-	-	-	-
Perched	FW	75	100	82.39	89.70	86.04	50	-	-	-	-	86.43	89.70	88.07	50	85.33	87.06	86.20	100
	MGW	50	75	70.47	73.01	71.74	50	69.77	72.01	70.89	100	72.02	73.30	72.66	50	-	-	-	-
	SGW	10	50	-	-	-	-	-	-	-	-	-	-	-	-	-	-	-	-
	SW	0	10	-	-	-	-	-	-	-	-	-	-	-	-	-	-	-	-
Saline	FW	75	100	75.54	87.80	75.85	41.67	76.80	83.10	79.95	40	76.71	86.91	85.61	80	76.45	84.24	81.16	100
	MGW	50	75	59.15	69.33	65.14	58.33	68.25	74.47	71.70	60	70.36	70.40	70.38	20	-	-	-	-
	SGW	10	50	-	-	-	-	-	-	-	-	-	-	-	-	-	-	-	-
	SW	0	10	-	-	-	-	-	-	-	-	-	-	-	-	-	-	-	-
Confined	FW	75	100	75.36	94.08	83.47	95.45	76.84	90.94	86.13	86.67	79.35	86.23	82.54	75	77.68	87.47	84.54	69.23
	MGW	50	75	63.73	63.75	63.74	4.55	66.54	71.64	69.9	13.33	69.51	74.64	72.67	25	63.33	70.71	64.40	30.76
	SGW	10	50	-	-	-	-	-	-	-	-	-	-	-	-	-	-	-	-
	SW	0	10	-	-	-	-	-	-	-	-	-	-	-	-	-	-	-	-

FW freshwater, *MGW* mixed groundwater, *SGW* saline groundwater, *SW* seawater

In 2011, the confined aquifer, characterized by the predominance of the Ca $-$HCO$_3$ type in comparison to other available types (mixed Ca–Mg–Cl, Na–Cl), indicates minimal influence from saltwater intrusion. The cause behind this phenomenon is the overexploitation of groundwater through pumping wells and rise of the saltwater arch, acting as the bedrock in this aquifer. Consequently, the intrusion phenomenon is observed locally in some parts of the aquifer. The trend of decreasing the percentage of Ca $-$HCO$_3$-type samples and increasing the percentage of Na–Cl-type samples during 2014 to 2020 suggests an escalation in intrusion, attributable to the factors outlined in 2011 (Fig. 16).

The investigation of the GQI_{SWI} index in four aquifers and drawing its spatiotemporal distribution (Figs. 17 and 18) over 10 years reveals that a sample is not included in the group of seawater and saline groundwater (Table 8). Compared to the modified Piper diagram results, the groundwater samples of each aquifer are classified into two groups: freshwater and mixed ground water.

In unconfined aquifer, with the improvement of the water quality, the composition of freshwater has experienced an increasing trend of 79.17, 66.67, 78.26, and 82.6% during the 4 years (2011, 2014, 2017, and 2020). Also, in this aquifer, with the gradual reduction of sea saltwater intrusion, the chemical type of 20.83, 33.33, 21.74, and 17.40% of the samples was changed to mixed groundwater (Table 8; Fig. 17).

The saline aquifer affected by the freshwater of the Alborz irrigation network, which feeds the aquifers, has led to the creation of freshwater composition in 41.67, 40, 80, and 100% of the samples during 4 years, respectively. The positive effects of constructing irrigation networks on increasing the groundwater table level have also been confirmed in the Ghobadian et al. (2014) and YariPilmaraei et al. (2011) studies. Overexploitation from deep wells has led to saltwater rising from the lower layers and the intensification of saltwater intrusion phenomenon in the confined aquifer. This led to a decrease in the composition of freshwater from 95.45% in 2011 to 69.23% in 2020 in the samples of this aquifer. Therefore, the intrusion of poor-quality water available in the saltwater arch led to an increase in the composition of mixed groundwater from 4.55% in 2011 to 30.76% in 2020 (Fig. 18).

Investigating the spatial distribution of the qualitative composition of samples using the GQI_{SWI} index shows that the process of saltwater intrusion in all aquifers has been an increasing trend from 2011 to 2014. This trend is attributed to the rising utilization of groundwater for agricultural purposes.

The process of increasing salinity and reducing the water quality of unconfined, perched, and saline aquifers affected by the establishment of the Alborz water supply network to allocate surface water for agricultural purposes from 2014 to 2020 has largely stopped and led to the improvement of the quality conditions of the mentioned aquifers. While in the confined aquifer, this trend is not true, and from 2014 to 2020, an increase in the mixing, infiltration, and intrusion of saltwater can be seen. According to the obtained results, it can be found that although both methods (modified Piper diagram and GQI_{SWI} index) can indicate changes in groundwater quality, the modified Piper diagram demonstrates a higher degree of accuracy and detail in classifying the quality of groundwater compared to the GQI_{SWI} index.

## Assessment of the hydrochemical facies evolution using HFE-D

Generally, using methods such as the modified Piper diagram and calculating the GQI_{SWI} index, it is impossible to accurately identify the evolution sequence of hydrochemical facies during the process of intrusion and freshening. For this purpose, Gimenez-Forcada (2010) suggested that the HFE-D diagram can determine the evolution of the intrusion and freshening processes more accurately and comprehensively than other methods. This diagram is a graphical approach to finding hydrochemical facies and spatiotemporal dynamics of seawater intrusion processes in coastal aquifers (Giménez-Forcada 2019). The range of hydrochemical composition of aquifers expresses the difference in the evolution process of hydrochemical facies and the salinity potential of aquifers.

According to the HFE-D diagram, freshwater belongs to Ca $-$HCO$_3$/SO$_4$ type in the zone (13) (sub-stage "f$_4$"), and saline water belongs to the Na–Cl type in the zone (4) (sub-stage "i$_4$"). During the intrusion phase, primary freshwater (Ca–HCO$_3$/SO$_4$) in zone (13) (sub-stage "f$_4$") with Ca–Cl, MixCa–Cl, MixNa–Cl, and Na–Cl in the zone (16 and 8, 12, 4) (sub-stage "i$_3$" and "i$_4$") is replaced. While in the freshening phase, facies with Na–Cl type in the zone (4) (sub-stage "f$_1$") evolve to Na–HCO$_3$/SO$_4$, MixNa–HCO$_3$/SO$_4$, MixCa–HCO$_3$/SO$_4$, and Ca–HCO$_3$/SO$_4$ in the zone (13, 1, 5, 9) (sub-stage "f$_4$").

In order to evaluate the chemical composition of the groundwater during the intrusion and freshening processes, the HFE diagram was drawn for all four aquifers in the GH.-J. plain (Fig. 19). Also, based on this diagram, the number and percentage of facies in different aquifers were identified and presented in Table 9. In this evaluation, the samples from the years 2011, 2014, 2017, and 2020 were examined to assess the long-term changes that were not discernible through the modified Piper chart method and the GQI_{SWI} index.

Most of the groundwater samples during these 10 years belong to the facies along the mixing line (13–10–7–4), which indicates simple mixing of fresh and salt water with little or no effect of cation exchanges. The position of the conservative mixing line (CML) in the four aquifers (Fig. 19) is different from the standard diagram presented by Gimenez-Forcada (2010) and Giménez-Forcada (2014). It

Fig. 19 HFE-D to identify salt-
water intrusion in unconfined,
perched, and saline aquifers in
2011 (**a**), 2014 (**b**), 2017 (**c**),
and 2020 (**d**) and in confined
aquifer in 2011 (**e**), 2014 (**f**),
2017 (**g**), and 2020 (**h**)
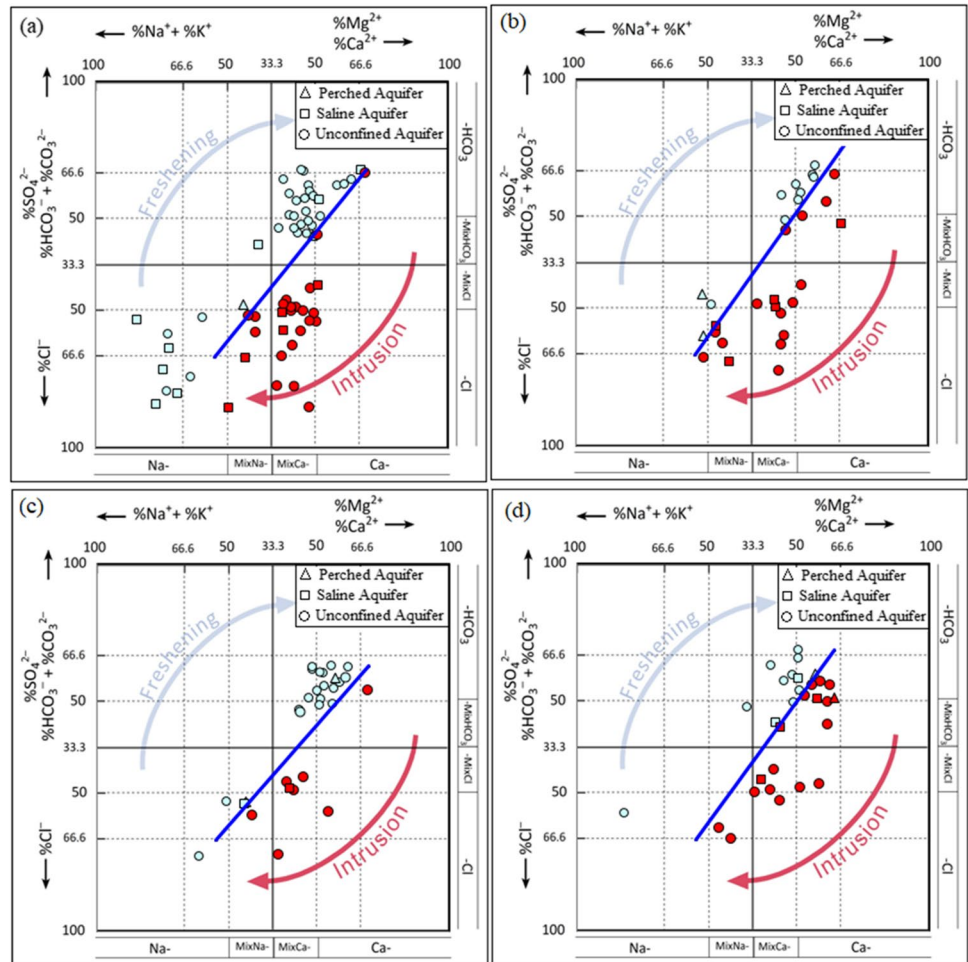
should be noted that the position of this line depends on the selected freshwater end-member composition in a specific case study.

The mixing line in the diagram related to the unconfined aquifer in 2011 (Fig. 19a) is placed in the intrusion phase, which shows the salinity conditions prevail in this aquifer. The results of HFE-D (Table 9) show that in the unconfined aquifer in 2011, approximately 54% of the samples are in the freshening phase of the HFE chart and are plotted above the FW-SW mixing line. This shows that the intrusion phase is progressing, and freshwater recharge has been able to repel the intrusion phase partially. The observation of the two dominant types, MixCa–HCO$_3$/SO$_4$ and MixCa–Cl, in the aquifer confirms that this aquifer is affected by two factors: precipitation and saltwater infiltration.

The position of this mixing line in 2014 is transferred to the position of the mixing line of the standard Gime'nez-Forcada diagram, which indicates the sweetening of groundwater compared to 2011 under the influence of freshwater recharge (Fig. 19b). In 2014, although almost 65% of the samples in the intrusion phase are plotted below the FW-SW mixing line, two water types of Ca–HCO$_3$/SO$_4$ and MixCa–Cl have

increased significantly compared to 2011. It shows that the aquifer is reviving itself by feeding through the fresh surface water that entered the plain with the establishment of the Alborz water supply network. Also, the freshening process by direct cation exchange reactions is progressing and overcoming the intrusion phase. This result is consistent with the findings of shahnazari et al. (2018), which confirms the increase in the groundwater table level after implementing of the Alborz irrigation network construction plan.

In 2017, the mixing line was again transferred to the intrusion phase, but the percentage of freshening phase samples above the FW–SW mixing line has increased to 68% (Fig. 19c; Table 9). Also, the number of samples from zone (13) with Ca–HCO$_3$/SO$_4$ type has increased, and the samples from zone (12) with MixCa–Cl type have been transferred to zones (11 and 9) with MixCa–MixCl and MixCa–HCO$_3$/SO$_4$ type. The chemical evolutions observed indicate the freshwater recharge of the aquifer, the continuation of the freshening process, and direct cation exchange reactions within the aquifer. These changes are attributed to the influence of receiving fresh surface water from the Alborz water supply network.

Fig. 19 (continued)
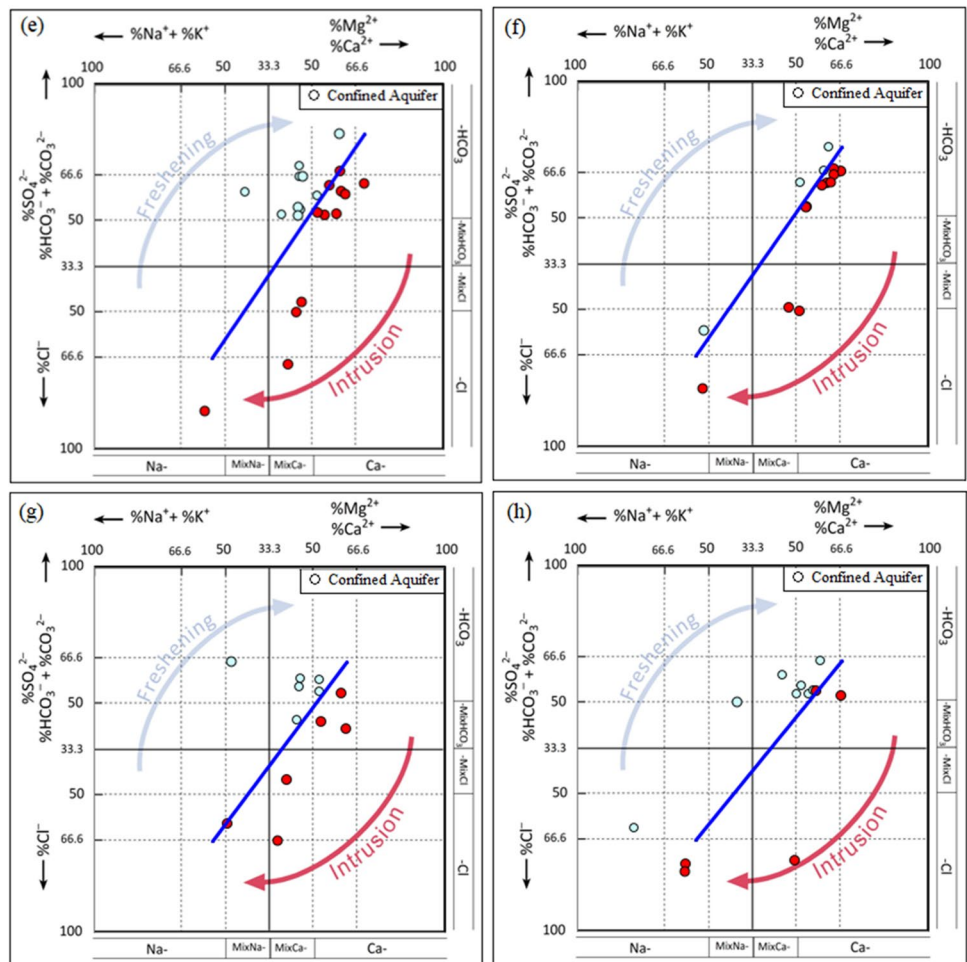
In 2020, the percentage of intrusion phase samples increased again and reached 65%, which reflects the predominance of the intrusion phase and reverse cation exchanges (Fig. 19d). The dominant types of aquifer in this year are similar to 2017, with the distinction that the number of samples of zone (13) with $Ca - HCO_3/SO_4$ type has decreased, while zones (9 and 11) with MixCa–MixCl and MixCa $-HCO_3/SO_4$ types have seen an increase. This could indicate a mixing and intrusion process.

In 2011, in the confined aquifer, 55% of the samples were plotted below the FW–SW mixing line and in the intrusion phase of the HFE diagram. The observation of the two dominant types of $Ca - HCO_3/SO_4$ and $MixCa–HCO_3/SO_4$ in zones (13) and (9) indicates that although the water of this aquifer has been good quality in 2011, but the intrusion phase and reverse cation exchange is progressing in this aquifer (Fig. 19e; Table 9).

In 2014, approximately 86% of the samples in the intrusion phase were plotted below the FW–SW mixing line, which shows the progress of the intrusion phase. Also, the dominant type this year is the $Ca - HCO_3/SO_4$. According to the drawn HFE-D diagram, it can be seen that one sample

in the zone (11) with MixCa–MixCl type, one sample in the zone (16) with Ca–Cl type, and finally, two samples in the zone (4) with Na–Cl type are located (Fig. 19f). This expresses the progression of the intrusion phase and the inverse cation exchanges as locally. Considering that the confined aquifer is located in the southern part of the plain and far from the Caspian Sea, the cause of the intrusion cannot be interference with the Caspian Sea. Due to the over-exploitation of the deep wells and the rising of the saltwater arch that plays the bedrock in the aquifers of the GH.-J. plain, this aquifer has become locally saline.

In 2017, the percentage of samples above and below the mixing line reached 50 (Table 9), indicating the equilibrium between the two phases of intrusion and freshening. The dominant type this year remains the $Ca–HCO_3/SO_4$ zone type (13), but the percentage of samples of this type has significantly decreased compared to 2014. The transfer of several samples from the zone (13) with $Ca–HCO_3/SO_4$ type to zone (14) with $Ca–Mix\ HCO_3/Mix\ SO_4$ type indicates the progress of the intrusion process and the reverse cation exchange resulting from excessive extraction from deep wells and localized saltwater upconing. Furthermore,

Table 9 Hydrochemical facies of GH.-J. groundwater samples based on the HFE diagram

Type of aquifer	HFE-D facies	Percent of HFE facies for GH.-J. in groundwater samples							
		2011		2014		2017		2020	
		No. of sample	%	No	%	No	%	No	%
Unconfined Aquifer	Na–Cl	3	6.12	1	4.17	2	7.70	1	4.35
	MixNa–Mix HCO$_3$/Mix SO$_4$	-	-	-	-	-	-	1	4.35
	MixNa–MixCl	-	-	1	4.17	-	-	-	-
	MixNa–Cl	3	6.12	2	8.33	1	3.85	2	8.70
	MixCa–HCO$_3$/SO$_4$	12	24.49	1	4.17	3	11.52	3	13.04
	MixCa–Mix HCO$_3$/Mix SO$_4$	7	14.29	2	8.33	2	7.70	1	4.35
	MixCa–MixCl	6	12.25	2	8.33	3	11.52	3	13.04
	MixCa–Cl	9	18.36	4	16.66	1	3.85	1	4.35
	Ca–HCO$_3$/SO$_4$	7	14.29	9	37.50	11	42.31	7	30.42
	Ca–Mix HCO$_3$/Mix SO$_4$	1	2.04	1	4.17	2	7.70	2	8.70
	Ca–MixCl	-	-	1	4.17	-	-	2	8.70
	Ca–Cl	1	2.04	-	-	1	3.85	-	-
Saline Aquifer	Na–Cl	6	54.54	-	-	-	-	-	-
	MixNa–Cl	1	9.09	2	40	1	50	-	-
	MixCa–Mix HCO$_3$/Mix SO$_4$	1	9.09	-	-	-	-	2	40
	MixCa–MixCl	-	-	1	20	1	50	1	20
	MixCa–Cl	2	18.19	1	20	-	-	-	-
	Ca–HCO$_3$/SO$_4$	-	-	-	-	-	-	2	40
	Ca–Mix HCO$_3$/Mix SO$_4$	-	-	1	20	-	-	-	-
	Ca–MixCl	1	9.09	-	-	-	-	-	-
Perched Aquifer	Na–MixCl	-	-	1	50	-	-	-	-
	Na–Cl	-	-	1	50	-	-	-	-
	MixNa–MixCl	1	50	-	-	-	-	-	-
	MixNa–Cl	-	-	-	-	1	50	-	-
	MixCa–Mix HCO$_3$/Mix SO$_4$	1	50	-	-	-	-	-	-
	Ca–HCO$_3$/SO$_4$	-	-	-	-	1	50	2	100
Confined Aquifer	Na–Cl	1	4.55	2	14.30	-	-	3	23.06
	MixNa–HCO$_3$/SO$_4$	1	4.55	-	-	1	8.33	1	7.70
	MixNa–Cl	-	-	-	-	1	8.33	-	
	MixCa–HCO$_3$/SO$_4$	7	31.81	-	-	2	16.68	1	7.70
	MixCa–Mix HCO$_3$/Mix SO$_4$	-	-	-	-	1	8.33	-	-
	MixCa–MixCl	1	4.55	1	7.14	1	8.33	-	-
	MixCa–Cl	2	9.09	-	-	1	8.33	1	7.70
	Ca–HCO$_3$/SO$_4$	10	45.45	10	71.42	3	25	7	53.84
	Ca–Mix HCO$_3$/Mix SO$_4$	-	-	-	-	2	16.67	-	-
	Ca–Cl	-	-	1	7.14	-	-	-	-

transferring the composition of a sample from zone (4) with Na–Cl type to zone (5) with MixNa–HCO$_3$/SO$_4$ type and a sample from zone (16) with Ca–Cl type to zone (9) with MixCa–HCO$_3$/SO$_4$ type reflects the freshening conditions and direct cation exchange caused by fresh surface water feeding from limited recharge areas of the confined aquifer (Fig. 19g).

In 2020, the percentage of samples above the FW–SW mixing line will reach 62% (Table 9), which indicates the predominance of the freshening phase. Also, by doubling the percentage of samples located in the zone (13) with Ca–HCO$_3$/SO$_4$ type compared to 2017, the effect of feeding from the Alborz water supply network can be seen. It is worth noting that due to the limited feeding area of the confined aquifer compared to the unconfined aquifer, the effect of fresh surface water percolation is observed with more delay than the unconfined aquifer. Observing samples with MixNa–HCO$_3$/SO$_4$ type (zone 5) and MixCa–HCO$_3$/SO$_4$

type (zone 9) indicates the progress of the freshening process and direct cation exchanges. On the other hand, the observation of MixCa–Cl type (zone 12) and the Na–Cl type (zone 4) proves the progress of the intrusion process and the reverse cation exchange locally (Fig. 19h).

In the saline aquifer, the lack of sufficient freshwater recharge has caused the intrusion phase to dominate in this aquifer during 2011–2020 (The position of the mixing line in HFE-D (Fig. 19a–d) further corroborates this situation). In 2011, the dominant type of the aquifer was Na–Cl (zone 4), which indicates the complete salinization due to the intrusion process and reverse cation exchanges. The samples taken from this aquifer by Heidari Cherati (2020) also prove that this area has been affected by seawater intrusion due to excessive harvesting for agricultural purposes.

The transfer of the hydrochemical composition of the samples from zone (4) with Na–Cl type in 2011 to zone (8) with MixNa–Cl type in 2014 shows the mixing of saltwater with freshwater fed to the aquifer under the influence of the WSNA and the progress of the freshening phase in the saline aquifer. Finally, in 2020, with the continuation of the freshening process, the samples have shifted to zones (10) and (13) with the combination of MixCa–Mix HCO_3/Mix SO_4 and Ca − HCO_3/SO_4 (freshwater), indicating the progress of freshening and direct cation exchange.

The samples in the perched aquifer in 2011, similar to the unconfined aquifer, are located above the FW–SW mixing line and in zones (7) and (10) with the combination of MixNa–MixCl and MixCa–Mix HCO_3/Mix SO_4. This indicates that the aquifer is affected by the simple mixing of fresh and salt water with little or no effect of cation exchanges.

With the establishment of the WSNA in 2013, the freshwater front in the unconfined aquifer has become stronger and has moved in the direction of the hydraulic gradient from the south to the north (Caspian Sea). As a result, it causes a mixing of the freshwater of the perched aquifer with the saltwater of the saline aquifer. Therefore, as a result of intrusion and reverse cation exchanges, the Na–Cl and Na–MixCl types emerged in 2014.

In 2017, the perched aquifer altered its composition to MixNa–Cl (zone 8) and Ca −HCO_3/SO_4 (freshwater) (zone 13) by continuing to feed unconfined and saline aquifers with fresh surface waters and the progress of the freshening phase. This indicates the strengthening of the freshwater front and the repulsion of the saltwater from the perched aquifer. From 2017 to 2020, the freshening process continued so that in 2020, only Ca −HCO_3/SO_4 (zone 13) was observed in this aquifer. Indeed, it can be observed that the freshening process and direct cation exchanges are progressing in this aquifer located near the sea.

In order to evaluate the spatiotemporal distribution of hydrochemical facies using the sub-stages of the HFE-D

diagram, the sampling points were ranked according to Table 2. Vulnerability maps of aquifers to saltwater intrusion were then created based on HFE-D for four selected years. The data were transformed into zoning maps using the kriging interpolation method. The spatiotemporal variations of freshening and intrusion conditions in four aquifers have been shown in Fig. 20. The relationship between coastal aquifers and seawater is a dynamic balance that relies on variations in recharge and discharge variations over time. This is evident in the boundary between freshening and intrusion depicted on the maps for each aquifer.

In 2011, within the unconfined aquifer, the boundaries between freshening and intrusion phases expanded significantly, encompassing a substantial portion of the unconfined aquifer, a significant segment of the saline aquifer, and limited areas to the east of the perched aquifer. This expansion is attributed to the overexploitation of wells for agricultural purposes. Only a tiny area in the south and north of the plain has been spared from intrusion (Fig. 20a). This shows that the feeding of the aquifer through precipitation and runoff was not enough for freshening to overcome intrusion. Also, considering that the Talar and Siah rivers feed the aquifer in the southern part and drain the aquifer in the middle and northern parts of the plain (Fig. 21); therefore, the evolution of hydrochemical facies in the unconfined aquifer is affected by this phenomenon. Consequently, freshening prevails in the southern part of the aquifer.

It should be noted that the aquifer drainage by the mentioned rivers in the area of the saline aquifer can be considered a factor in intensifying the intrusion phase in this part of the aquifer. Therefore, the zone of freshening and intrusion along the course of the rivers indicates the effective hydraulic connection between the river and these aquifers. According to the surface water quality data obtained from the MRWC, the type of water in Talar and Siah Roud rivers exhibits a transition in composition. Upstream, it is characterized as calcium bicarbonate, in the middle as calcium sulfate, and downstream and close to the coastline as a combination of calcium chloride and sodium chloride, respectively. Additionally, throughout the study period, the EC and TDS values of these rivers are the lowest in the upstream, increase in the middle of the plain, and show a significant increase in downstream of the plain.

In 2014, the process of evolution of the hydrochemical facies of the unconfined aquifer has progressed in the direction of freshening due to freshwater recharge from the WSNA. The freshwater front from the south of the plain has strengthened and pushed the boundary between the two phases of freshening and intrusion. Consequently, this boundary in the unconfined aquifer has extended to areas near the center of the plain. Also, the freshwater front from the south of the plain and in the direction of the hydraulic gradient exerted pressure on the saltwater of the
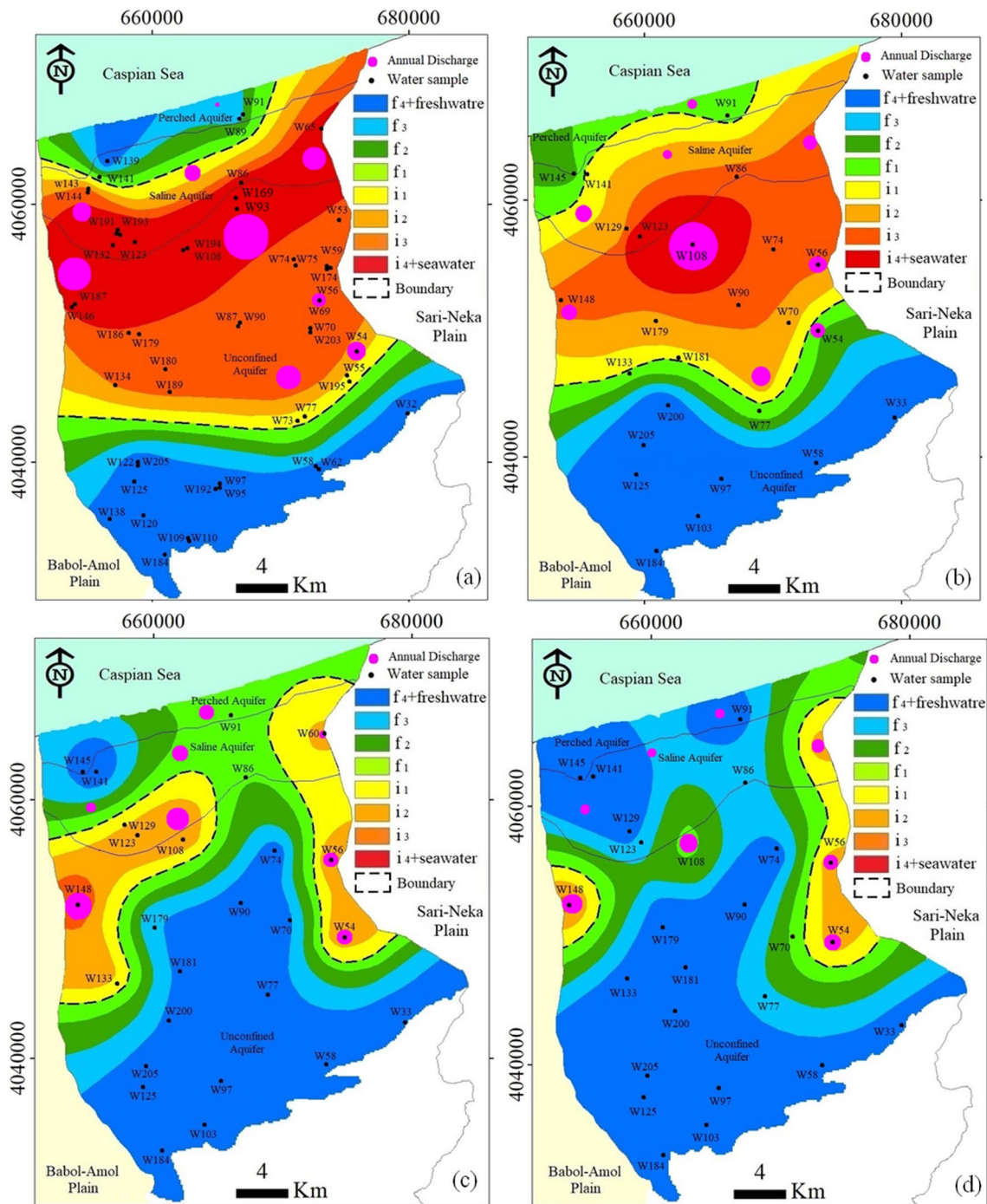
Fig. 20 Spatial distribution of hydrochemical facies sub-stages in 2011, 2014, 2017, and 2020 in perched, saline, and unconfined aquifers (**a**, **b**, **c**, **d**) and confined aquifer (**e**, **f**, **g**, and **h**). Larger and small pink circles indicate more and less annual discharge, respectively

saline aquifer and brought the saltwater front to the perched aquifer. As a result, it can be seen that although the quality of unconfined and saline aquifers improved compared to 2011, the quality of perched aquifer decreased. These results show the evolution of the hydrochemical facies in the unconfined aquifer influenced by freshwater recharge (Fig. 20b).

The impact of continuous and increased freshwater recharge on the evolution of hydrochemical facies and the enhancement of the water quality in unconfined, saline, and perched aquifers in 2017 and 2020 can be seen in Fig. 20c, d. So that in 2017, with the increase of freshwater recharge, the strong freshwater front moved in the direction of the hydraulic gradient from the south to the north of the plain
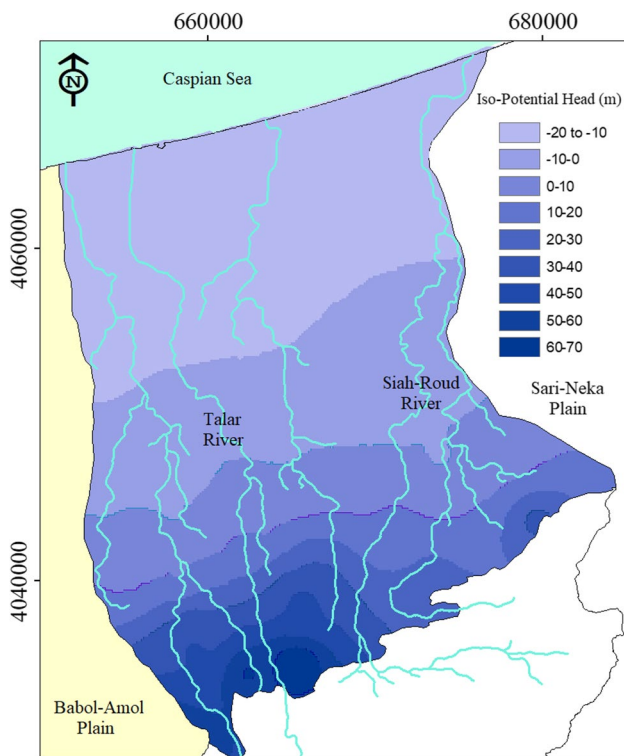
Fig. 21 Groundwater table level map of the unconfined aquifer in 2020

and split the saltwater zone. During this year, the effects of the intrusion phase are observed only in parts of the east and southwest of the saline aquifer and in the eastern and northwestern areas of the unconfined aquifer. Ultimately, the freshening phase prevails in the perched aquifer.

The increase of freshwater recharge in 2020 and its effect on the strengthening of the freshwater front, coupled with the retreat of the saltwater front in the eastern and western parts of the plain, affirm that the hydrochemical facies pattern in these three aquifers is more influenced by recharge factor and factors. Other factors such as aquifer lithology and the extent of groundwater drawdown appear to be less critical (Fig. 20d).

The hydrochemical facies pattern of the confined aquifer, situated in the southern area of the plain beneath the unconfined aquifer, is more responsive to fluctuations in groundwater levels caused by excessive pumping from deep wells in this aquifer than to the amount of recharge. This could be attributed to the limited extent of the recharge area for this aquifer and its considerable distance from the primary recharge source, predominantly recharged from the heights of the southern border of the plain.

In 2011 and 2014, the confined aquifer was balanced (Fig. 20e, f), and no traces of intrusion can be observed in it. In 2017, the intrusion phase was observed in two distinct areas, one in the east and the other in the west of the aquifer.

Notably, these areas coincide with locations characterized by intensive pumping, where there is a scarcity of fresh surface water for agricultural and domestic use. Despite the increase in rainfall and freshwater recharge from the Alborz water supply network in the current year, the intrusion phase prevails in the western and eastern parts of the study area. This dominance is attributed to the substantial drawdown in groundwater levels resulting from the excessive extraction of deep wells and the rising of the saltwater arch in the confined aquifer (Fig. 20g).

The increasing trend of the intrusion phase continues in the western and eastern parts of the studied area in 2020 (Fig. 20h). Therefore, it seems that the confined aquifer lacks direct local recharge compared to the other three aquifers. The confirmation of these findings is evident in the HFE-D diagram, the position of the mixing line, the percentage of samples in each zone, and the sub-stage in all four aquifers as depicted in Fig. 20.

The role of lithostratigraphy formations in groundwater hydrochemical evolution

The GH.-J. catchment area is composed chiefly of limestone, marl, and dolomite formations in the highlands and alluvial fans in the plain, which consist of coarse-grained and permeable sediments. Towards the center of the plain, fine-grained sand, silty and clay sediments (new Caspian sediments) and below that, the sediments of the Apsheron formation are composed of clay, marl, unhardened sand, and conglomerate. According to the lithostratigraphy and geology of the case study, the chemical composition of the groundwater of GH.-J. plain can be described from the recharge zone to the discharge area.

In the recharge zone, the type of water is $Ca-HCO_3$ due to the dissolution of carbonate minerals, with its quantity decreasing from the south to the north of the plain. In the middle part, the water type transitions to more Ca–Mg–Cl. The hydrochemical evolution is influenced by two main factors: the infiltration of saline water from the fossil saline aquifer and the process of cation exchange between groundwater and the alluvial layers containing clay. In this section, due to the absence of evaporite minerals, the dissolution process has not played a role in the evolution of groundwater hydrochemistry. At the end of the middle section, the water type shifts to Na–Cl. This is attributed to both the direct infiltration of saline water from the fossil saline aquifer and the exchange of cations between the groundwater and alluvial layers containing clay in this area, resulting in the formation of the saline aquifer. In the final part of the plain and the vicinity of the Caspian Sea, the placement of clay lenses on the alluvial layers has given rise to a perched aquifer with Ca–HCO3 water type. The hydrochemical composition of this aquifer has changed over the years, influenced by factors

such as the infiltration of salty seawater, cation exchanges, and agricultural activities. The results obtained from the scatter diagrams, PCA, saturation index, the modified Piper diagram, and HFE-D methods confirm the aforementioned findings.

Conclusions

The evolution of the hydrochemical facies governing the multilayered aquifer of GH.-J. coastal plain as a result of the Caspian sea saltwater intrusion and other saltwater sources were analyzed using combined methods. Based on this, the most important reasons for the salinity of aquifers and variations in its quality can be summarized as follows:

- The results of PCA analysis shows that the primary factors of salinity in the unconfined aquifer are geogenic processes, hydrogeochemical exchange between the aquifer and the Caspian Sea as a result of seawater intrusion, and fossil saline waters trapped between sediments. The second influential factor, confirmed by the increase in NO_3^- concentration, is the excessive development of agricultural lands, increasing the use of nitrogenous urea fertilizer, and the significant feeding of the aquifer by the resulting effluents. It should be noted that the increase in the Na/Cl ratio indicates the development of anthropogenic activities in creating aquifer pollution as a result of direct cation exchanges. Urban sewage and hydrogeochemical processes with natural origin have also been effective in this qualitative degradation of the aquifer. The analysis of the evolution of hydrochemical facies in the unconfined aquifer indicates that the establishment of the water supply network of Alborz Dam has significantly contributed to reducing the infiltration rate of saltwater from the sea and the underlying rock into the unconfined aquifer.
- In the saline aquifer, the results from the HFE-D diagram indicate the predominance of the intrusion phase over the freshening due to insufficient freshwater recharge throughout the four investigated time periods. The important factor of the salinity of this aquifer is the direct effect of intrusion and reverse cation exchanges due to geogenic factors and hydrogeochemical processes governing the aquifer. Similar to the unconfined aquifer, the establishment of the Alborz water supply network has a positive impact on this aquifer, leading to a significant decrease in salinity and an improvement in the quality of groundwater. In the saline aquifer of GH.-J. plain, under the influence of surface water feeding, the type of water changed from Na–Cl and Mixed Ca–Mg–Cl in 2011 to Mixed Ca–Mg–Cl and freshwater in 2020.

- In the northern parts of the plain and near the shores of the Caspian Sea, there is a perched aquifer of freshwater. Despite its proximity to the sea, the alluvial layer's placement on the clay lenses has ensured the containment of freshwater throughout the years. The mixed groundwater composition, as assessed through the GQI_{SWI} index and Piper diagram, displaying MixNa–MixCl and MixCa–Mix HCO_3/Mix SO_4 composition, indicates that this aquifer is influenced by the simple mixing of fresh and salt water with little or no impact from cation exchanges. The trend of spatiotemporal changes of the hydrogeochemical facies of this aquifer is similar to the unconfined aquifer. This indicates the reinforcement of the freshwater front and the retreat of the saltwater front from the perched aquifer due to the infusion of freshwater from the Alborz network.
- In the confined aquifer, saltwater and freshwater intrusions are seen. The first factor of this phenomenon is the geological processes due to the rising of fossil saline waters in the bedrock of this aquifer due to excessive exploitation of deep wells. The second reason is the reverse cation exchange process, human activities, and the use of nitrate-containing chemical fertilizers, which confirms the results of HFE-D. It should be noted that the intrusion phenomenon in this aquifer is not influenced by the sea, given its considerable distance from the coastline.

The findings showed that the simultaneous analysis of the results of statistical methods, the developed indicators in the modified Piper diagram, and the use of the HFE-D diagram is very effective in identifying the phenomenon of the interaction between salt and freshwater in coastal aquifers with marine or non-marine origin. The developed methodology can also unveil the reasons behind exchange processes and the concealed knowledge within them, shedding light on the factors causing changes in the spatiotemporal behavior of the hydrogeochemical facies governing the coastal aquifers. The obtained results can be considered as a foundation for developing both quantitative and qualitative policies for the operational management of coastal aquifers. These policies aim to remediate, protect, and efficiently manage groundwater resources, particularly in the coastal aquifers under the risk of saltwater intrusion.

Author contribution Software, methodology, investigation, and writing—original draft preparation, Tahereh Azari; conceptualization and methodology, validation, investigation, review, and editing, agreed to the published version of the manuscript, Mahmoud Mohammad Rezapour Tabari.

Data availability Not applicable.

Declarations

Ethics approval Not applicable.

Consent to participate Not applicable.

Consent for publication Not applicable.

Conflict of interest The authors declare no competing interests.

References

Abba S, Benaafi M, Usman A, Ozsahin DU, Tawabini B, Aljundi IH (2023) Mapping of groundwater salinization and modelling using meta-heuristic algorithms for the coastal aquifer of eastern Saudi Arabia. Sci Total Environ 858:159697. https://doi.org/10.1016/j.scitotenv.2022.159697

Abd-Elaty I, Javadi AA, Abd-Elhamid H (2021) Management of saltwater intrusion in coastal aquifers using different wells systems: A case study of the Nile Delta aquifer in Egypt. Hydrogeol J 29:1767–1783. https://doi.org/10.1007/s10040-021-02344-w

Amiri V, Nakhaei M, Lak R, Kholghi M (2015) Assessment of seasonal groundwater quality and potential saltwater intrusion: a study case in Urmia coastal aquifer (NW Iran) using the groundwater quality index (GQI) and hydrochemical facies evolution diagram (HFE-D). Stoch Env Res Risk Assess 30(5):1473–1484. https://doi.org/10.1007/s00477-015-1108-3

Amiri V, Bhattacharya P, Nakhaei M (2021) The hydrogeochemical evaluation of groundwater resources and their suitability for agricultural and industrial uses in an arid area of Iran. Groundw Sustain Dev 12:100527. https://doi.org/10.1016/j.gsd.2020.100527

Amiri-Bourkhani M, Khaledian MR, Ashrafzadeh A, Shahnazari A (2017) The temporal and spatial variations in groundwater salinity in Mazandaran Plain, Iran, during a long-term period of 26 years. Geofizika 34(1):119–139. https://doi.org/10.15233/gfz.2017.34.4

APHA (2005) Standard methods for the examination of water and wastewater, 21st edn. American Public Health Association/American Water Works Association/Water Environment Federation, Washington DC

Appelo CAJ, Postma D (2004) Geochemistry, groundwater and pollution. CRC Press

Asare A, Appiah-Adjei EK, Ali B, Owusu-Nimo F (2021) Assessment of seawater intrusion using ionic ratios: the case of coastal communities along the Central Region of Ghana. Environmental Earth Sciences 80(8). https://doi.org/10.1007/s12665-021-09601-x

Barkat A, Bouaicha F, Bouteraa O, Mester T, Ata B, Balla D, Rahal Z, Szabó G (2021) Assessment of complex terminal groundwater aquifer for different use of Oued Souf Valley (Algeria) using multivariate statistical methods, geostatistical modeling, and water quality index. Water 13(11):1609. https://doi.org/10.3390/w13111609

Biswas T, Pal SC, Saha A (2023) Hydro-chemical assessment of coastal groundwater aquifers for human health risk from elevated arsenic and fluoride in West Bengal. India Marine Pollution Bulletin 186:114440. https://doi.org/10.1016/j.marpolbul.2022.114440

Carol ES, Kruse EE (2012) Hydrochemical characterization of the water resources in the coastal environments of the outer Río de la Plata estuary, Argentina. J S Am Earth Sci 37:113–121. https://doi.org/10.1016/j.jsames.2012.02.009

Carol E, Kruse E, Mas-Pla J (2009) Hydrochemical and isotopical evidence of ground water salinization processes on the coastal plain of Samborombón Bay. Argentina Journal of Hydrology 365(3):335–345. https://doi.org/10.1016/j.jhydrol.2008.11.041

Chandra Pal S, Towfiqul Islam ARM, Chakrabortty R, Islam MS, Saha A, Shit M (2022) Application of data-mining technique and hydro-chemical data for evaluating vulnerability of groundwater in Indo-Gangetic Plain. J Environ Manage 318:115582. https://doi.org/10.1016/j.jenvman.2022.115582

Chitsazan M, Mohammad Rezapour Tabari M, Eilbeigi M (2017) Analysis of temporal and spatial variations in groundwater nitrate and development of its pollution plume: a case study in Karaj aquifer. Environmental Earth Sciences 76(11). https://doi.org/10.1007/s12665-017-6677-7

Desai BI, Desai HS (2012) Assessment of water quality index for ground water with respect to salt water intrusion at Coastal Region of Surat City, Gujarat, India. J Environ Res Dev 7:607–621. https://doi.org/10.4236/jwarp.2017.92015

Dhar A, Datta B (2009) Saltwater intrusion management of coastal aquifers. I: linked simulation-optimization. J Hydrol Eng 14(12):1263–1272. https://doi.org/10.1061/(ASCE)HE.1943-5584.0000097

Elemile OO, Ibitogbe EM, Folorunso OP, Ejiboye PO, Adewumi JR (2021) Principal component analysis of groundwater sources pollution in Omu-Aran Community, Nigeria. Environmental Earth Sciences 80(20). https://doi.org/10.1007/s12665-021-09975-y

El-Fadel M, Tomaszkiewicz M, Adra Y, Sadek S, Abou Najm M (2014) GIS-based assessment for the development of a groundwater quality index towards sustainable aquifer management. Water Resour Manage 28(11):3471–3487. https://doi.org/10.1007/s11269-014-0683-2

Elgettafi M, Elmandour A, Himi M, Casas i Ponsatí A, Elhaouadi B, (2012) Messinian salinity crisis impact on the groundwater quality in Kert aquifer NE Morocco: hydrochemical and statistical approaches. Int J Water Res Environ Eng 4(11):339–351. https://doi.org/10.5897/IJWREE12.002

Geological Survey of Iran (2003) A geological map with a scale of 1:100000 and a topographic map of 1: 50000 and 1: 25000. National Geoscience Database of Iran. https://www.ngdir.ir (In Persian)

Ghobadian R, Fattahi chaghabaki A, Zare M (2014) Studying the effects of Gavoshan Dam's irrigation and drainage network on groundwater of Miandarband Plain using GMS 6.5 model. J Water Res Agric 28(4):759–772 (In Persian)

Ghezelsofloo E, Raghimi M, Mahmoodlu MG, Rahimi-Chakdel A, Khademi SMS (2021) Saltwater intrusion in drinking water wells of Kordkuy, Iran: an integrated quantitative and graphical study. Environmental Earth Sciences 80(16). https://doi.org/10.1007/s12665-021-09843-9

Gholami V, Yousefi Z, Zabardast Rostami H (2009) Modeling of ground water salinity on the Caspian southern coasts. Water Resour Manage 24(7):1415–1424. https://doi.org/10.1007/s11269-009-9506-2

Ghosh S, Sarkar B, Islam A, Shit PK, Quesada-Román A, Gazi HAR (2022) Surface water and groundwater suitability for irrigation based on hydrochemical analysis in the Lower Mayurakshi River Basin. India Geosciences 12(11):415. https://doi.org/10.3390/geosciences12110415

Gimenez-Forcada E (2010) Dynamic of sea water interface using hydrochemical facies evolution diagram. Ground Water 48(2):212–216. https://doi.org/10.1111/j.1745-6584.2009.00649.x

Giménez-Forcada E (2014) Space/time development of seawater intrusion: a study case in Vinaroz coastal plain (Eastern Spain) using HFE-Diagram, and spatial distribution of hydrochemical facies. J Hydrol 517:617–627. https://doi.org/10.1016/j.jhydrol.2014.05.056

Giménez-Forcada E (2019) Use of the hydrochemical facies diagram (HFE-D) for the evaluation of salinization by seawater intrusion in the coastal Oropesa Plain: comparative analysis with the coastal Vinaroz Plain, Spain. HydroResearch 2:76–84. https://doi.org/10.1016/j.hydres.2019.11.007

Giménez-Forcada E, Sánchez San Román FJ (2015) An Excel macro to plot the HFE-Diagram to identify sea water intrusion phases. Ground Water 53(5):819–824. https://doi.org/10.1111/gwat.12280

Golshan M, Colombani N, Mastrocicco M (2018) Assessing aquifer salinization with multiple techniques along the southern caspian sea shore (Iran). Water 10(4):348. https://doi.org/10.3390/w10040348

Guo Q, Zhao Y, Hu Z, Li M (2021) Contamination transport in the coastal unconfined aquifer under the influences of seawater intrusion and inland freshwater recharge-laboratory experiments and numerical simulations. Int J Environ Res Public Health 18(2):762. https://doi.org/10.3390/ijerph18020762

Hajji S, Allouche N, Bouri S, Aljuaid AM, Hachicha W (2021) Assessment of seawater intrusion in coastal aquifers using multivariate statistical analyses and hydrochemical facies evolution-based model. Int J Environ Res Public Health 19(1). https://doi.org/10.3390/ijerph19010155

Heidari Cherati S (2020) Geochemical evolution of groundwater in the alluvial aquifer of Qaemshahr - Juybar. Dissertation, Faculty of Earth Sciences, Shahrood University of Technology (In Persian)

Hem JD (1970) Study and interpretation of the chemical characteristics of natural water. U.S. Geological Survey, Reston, VA

Islam ARMT, Shen S, Haque MA, Bodrud-Doza M, Maw KW, Habib MA (2017) Assessing groundwater quality and its sustainability in Joypurhat district of Bangladesh using GIS and multivariate statistical approaches. Environ Dev Sustain 20(5):1935–1959. https://doi.org/10.1007/s10668-017-9971-3

Jahanshahi R, Zare M (2016) Hydrochemical investigations for delineating salt-water intrusion into the coastal aquifer of Maharlou Lake. Iran J African Earth Sci 121:16–29. https://doi.org/10.1016/j.jafrearsci.2016.05.014

Janardhana M, Khairy H (2019) Simulation of seawater intrusion in coastal aquifers: a case study on the Amol–Ghaemshahr coastal aquifer system, Northern Iran. Environmental Earth Sciences 78(24). https://doi.org/10.1007/s12665-019-8711-4

Kanagaraj G, Elango L, Sridhar SGD, Gowrisankar G (2018) Hydrogeochemical processes and influence of seawater intrusion in coastal aquifers south of Chennai, Tamil Nadu. India Environ Sci Pollut Res Int 25(9):8989–9011. https://doi.org/10.1007/s11356-017-0910-5

Kawo NS, Karuppannan S (2018) Groundwater quality assessment using water quality index and GIS technique in Modjo River Basin, central Ethiopia. J Afr Earth Sc 147:300–311. https://doi.org/10.1016/j.jafrearsci.2018.06.034

Kelepertzis E, Matiatos I, Botsou F, Antonopoulou C, Lappas I, Dotsika E, Chrastný V, Boeckx P, Karavoltsos S, Komárek M (2023) Assessment of natural and anthropogenic contamination sources in a Mediterranean aquifer by combining hydrochemical and stable isotope techniques. Sci Total Environ 858:159763. https://doi.org/10.1016/j.scitotenv.2022.159763

Khairy H, Janardhana MR (2021) Classification, hydrochemical characterization, and quality assessment of groundwater of coastal aquifer at Sari–Neka plain, Northern Iran. Environmental Earth Sciences 81(1). https://doi.org/10.1007/s12665-021-10115-9

Khairy H, Janardhana MR (2013) Hydrogeochemistry and quality of groundwater of coastal unconfined aquifer in Amol-Ghaemshahr plain, Mazandaran Province. Northern Iran Environ Earth Sci 71(11):4767–4782. https://doi.org/10.1007/s12665-013-2868-z

Klassen J, Allen D, Kirste D (2014) Chemical indicators of saltwater intrusion for the Gulf Islands. Final Report, Department of Earth Sciences, Simon Rfaser University, British Columbia

Kouzana L, Benassi R, Ben Mammou A, SfarFelfoul M (2010) Geophysical and hydrochemical study of the seawater intrusion in Mediterranean semi arid zones Case of the Korba coastal aquifer (Cap-Bon, Tunisia). J African Earth Sci 58(2):242–254. https://doi.org/10.1016/j.jafrearsci.2010.03.005

Kura NU, Ramli MF, Ibrahim S, Sulaiman WN, Zaudi MA, Aris AZ (2014) A preliminary appraisal of the effect of pumping on seawater intrusion and upconing in a small tropical island using 2D resistivity technique. Sci World J 2014:796425. https://doi.org/10.1155/2014/796425

Larsen F, Tran LV, Van Hoang H, Tran LT, Christiansen AV, Pham NQ (2017) Groundwater salinity influenced by Holocene seawater trapped in incised valleys in the Red River delta plain. Nat Geosci 10(5):376–381. https://doi.org/10.1038/ngeo2938

Le TTV, Lertsirivorakul R, Bui TV, Schulmeister MK (2020) An application of HFE-D for evaluating sea water intrusion in coastal aquifers of southern Vietnam. Ground Water 58(6):1012–1022. https://doi.org/10.1111/gwat.13022

Li Q, Zhang H, Guo S, Fu K, Liao L, Xu Y, Cheng S (2020) Groundwater pollution source apportionment using principal component analysis in a multiple land-use area in southwestern China. Environ Sci Pollut Res Int 27(9):9000–9011. https://doi.org/10.1007/s11356-019-06126-6

Mahlknecht J, Steinich B, Navarro de León I (2004) Groundwater chemistry and mass transfers in the Independence aquifer, central Mexico, by using multivariate statistics and mass-balance models. Environ Geol 45(6):781–795. https://doi.org/10.1007/s00254-003-0938-3

Mazandaran Regional Water Organization (2010) quantitative and qualitative measurement statistics of surface and groundwater in Ghaemshahr plain and other information and reports in the organization. Final Report, Iran Ministry of Energy (In Persian)

Meyer R, Engesgaard P, Sonnenborg TO (2019) Origin and dynamics of saltwater intrusion in a regional aquifer: combining 3-D saltwater modeling with geophysical and geochemical data. Water Resour Res 55(3):1792–1813. https://doi.org/10.1029/2018WR023624

Ministry of Jihad-e-Agriculture IFRI (2006) Investigation of harmful algal bloom in the southwestern Caspian Sea. Final report, Iranian Fisheries Research Institute (In Persian)

Jehad MoA (2020) Organization of research, education and extension of agriculture, Deputy of Agricultural Education, Agriculture landscape of Mazandaran Province (In Persian)

Moghimi H (2017) The study of processes affecting groundwater hydrochemistry by multivariate statistical analysis (case study: coastal aquifer of Ghaemshahr, NE-Iran). Open J Geol 7(06):830

Moghimi H, Kocak K, Ea N (2016) The study of Caspian Sea salt water intrusion to aquifer of Ghaem shahr plain. Ecology, Environment and Conservation 22(1):67–75

Mohammadi Arasteh S, Shoaei SM (2020) An assessment of the effects of excessive groundwater abstraction on the quality of groundwater resources of the Zanjan Plain, Iran. Environmental Earth Sciences 79(23). https://doi.org/10.1007/s12665-020-09268-w

Mohammed Siraj Ansari A, Saraswathi R (2022) Use of principal component analysis for parameter selection to compute water quality index and assessment of groundwater quality status: a case study of Sanganur Stream, Coimbatore City. J Geol Soc India 98(3):417–422. https://doi.org/10.1007/s12594-022-1994-1

Motevalli A, Moradi HR, Javadi S (2018) A comprehensive evaluation of groundwater vulnerability to saltwater up-coning and sea water intrusion in a coastal aquifer (case study: Ghaemshahr-juybar aquifer). J Hydrol 557:753–773. https://doi.org/10.1016/j.jhydrol.2017.12.047

Motevalli A, Moradi HR, Javadi S (2019) The effects of overexploliation and land use change on groundwater resources salinization using vulnerability concept in the Ghaemshahr-Juybar aquifer. Watershed Management Research Journal 32(3):2–20. https://doi.org/10.22092/WMEJ.2019.124558.1179

Mtoni Y, Mjemah IC, Bakundukize C, Van Camp M, Martens K, Walraevens K (2013) Saltwater intrusion and nitrate pollution in the coastal aquifer of Dar es Salaam. Tanzania Environ Earth Sci 70(3):1091–1111. https://doi.org/10.1007/s12665-012-2197-7

Nemati M, Tabari M, Hosseini SA, Javadi s (2022) Identification of factors affecting nitrate contamination in Ardabil plain aquifer using statistical methods. Water and Irrigation Management:-. https://doi.org/10.22059/jwim.2022.343545.995 (In Persian)

Nezhadnaderi M (2018) Management of seawater intrusion in coastal aquifers of Caspian Sea. Anthropogenic Pollution 2(1):48–58. https://doi.org/10.22034/AP.2018.538412

Nguyen BT, Nguyen TMT, Bach QV (2020) Assessment of groundwater quality based on principal component analysis and pollution source-based examination: a case study in Ho Chi Minh City. Vietnam Environ Monit Assess 192(6):395. https://doi.org/10.1007/s10661-020-08331-0

Parisi A, Alfio MR, Balacco G, Güler C, Fidelibus MD (2023) Analyzing spatial and temporal evolution of groundwater salinization through multivariate statistical analysis and hydrogeochemical facies evolution-diagram. Sci Total Environ 862:160697. https://doi.org/10.1016/j.scitotenv.2022.160697

Parkhurst DL, Appelo C (1999) User's guide to PHREEQC (Version 2): A computer program for speciation, batch-reaction, one-dimensional transport, and inverse geochemical calculations. Water-Resources Investigations Report 99(4259):312

Piper AM (1944) A graphic procedure in the geochemical interpretation of water-analyses. EOS Trans Am Geophys Union 25(6):914–928. https://doi.org/10.1029/TR025i006p00914

Pulido-Leboeuf P, Pulido-Bosch A, Calvache ML, Vallejos Á, Andreu JM (2003) Strontium, SO_4^{2-}/Cl^- and Mg^{2+}/Ca^{2+} ratios as tracers for the evolution of seawater into coastal aquifers: the example of Castell de Ferro aquifer (SE Spain). CR Geosci 335(14):1039–1048. https://doi.org/10.1016/j.crte.2003.08.004

Puls RW, Barcelona MJ (1996) Low-flow (minimal drawdown) groundwater sampling procedures. US Environmental Protection Agency, Office of Research and Development. https://semspub.epa.gov/work/HQ/174364.pdf

Sahour H, Gholami V, Vazifedan M (2020) A comparative analysis of statistical and machine learning techniques for mapping the spatial distribution of groundwater salinity in a coastal aquifer. Journal of Hydrology 591. https://doi.org/10.1016/j.jhydrol.2020.125321

Sarath Prasanth S, Magesh N, Jitheshlal K, Chandrasekar N, Gangadhar K (2012) Evaluation of groundwater quality and its suitability for drinking and agricultural use in the coastal stretch of Alappuzha District, Kerala. India Applied Water Science 2(3):165–175. https://doi.org/10.1007/s13201-012-0042-5

Sarkar B, Islam A, Majumder A (2021) Seawater intrusion into groundwater and its impact on irrigation and agriculture: evidence from the coastal region of West Bengal, India. Regional Studies in Marine Science 44. https://doi.org/10.1016/j.rsma.2021.101751

Shahnazari A, Ghorbani Z, GholamiSefidkohi MA, Janatrostami S (2018) Simulation of groundwater from Qaemshahr-Juibar catchment under performance of Alborz Irrigation and Drainage Network. Journal of Watershed Management Research 9(17):246–257. https://doi.org/10.29252/jwmr.9.17.246

Shin K, Koh D-C, Jung H, Lee J (2020) The hydrogeochemical characteristics of groundwater subjected to seawater intrusion in the Archipelago. Korea Water 12(6):1542. https://doi.org/10.3390/w12061542

Siddha S, Sahu P (2020) Status of seawater intrusion in coastal aquifer of Gujarat, India: a review. SN Applied Sciences 2:1726. https://doi.org/10.1007/s42452-020-03510-7

Singh A (2015) Managing the environmental problem of seawater intrusion in coastal aquifers through simulation–optimization modeling. Ecol Ind 48:498–504. https://doi.org/10.1016/j.ecolind.2014.09.011

Su H, Kang W, Xu Y, Wang J (2017) Assessing groundwater quality and health risks of nitrogen pollution in the Shenfu Mining Area of Shaanxi Province. Northwest China Exposure and Health 10(2):77–97. https://doi.org/10.1007/s12403-017-0247-9

Subramani T, Elango L, Damodarasamy S (2005) Groundwater quality and its suitability for drinking and agricultural use in Chithar River Basin, Tamil Nadu. India Environmental Geology 47(8):1099–1110. https://doi.org/10.1007/s00254-005-1243-0

Tabari MMR, Abyar M (2022) Development a novel integrated distributed multi-objective simulation-optimization model for coastal aquifers management using NSGA-II and GMS models. Water Resour Manage 36:75–102. https://doi.org/10.1007/s11269-021-03012-0

Tomaszkiewicz M, Abou Najm M, El-Fadel M (2014) Development of a groundwater quality index for seawater intrusion in coastal aquifers. Environ Model Softw 57:13–26. https://doi.org/10.1016/j.envsoft.2014.03.010

Tziritis E, Sachsamanoglou E, Aschonitis V (2023) Assessing groundwater evolution with a combined approach of hydrogeochemical modelling and data analysis: application to the Rhodope Coastal Aquifer (NE Greece). Water 15(2):230. https://doi.org/10.3390/w15020230

Xiong G, Zhu X, Wu J, Liu M, Yang Y, Zeng X (2023) Seawater intrusion alters nitrogen cycling patterns through hydrodynamic behavior and biochemical reactions: based on Bayesian isotope mixing model and microbial functional network. Sci Total Environ 867:161368. https://doi.org/10.1016/j.scitotenv.2022.161368

YariPilmaraei E, Shaeri Karimi S, Dadmehr R (2011) Reaction models of groundwater resource system in Zarineroud plain of the factor charging and discharging through irrigation and drainage network plain, 4th conference of Iran water resource management. Iran (In Persian), Tehran, pp 1–8

Zhang B, Zhao D, Zhou P, Qu S, Liao F, Wang G (2020) Hydrochemical characteristics of groundwater and dominant water–rock interactions in the Delingha Area, Qaidam Basin. Northwest China Water 12(3):836. https://doi.org/10.3390/w12030836